Original Research

Advances in Structural Engineering

Beneficial and detrimental impacts of soil-structure interaction on seismic response of high-rise buildings

Advances in Structural Engineering
2024, Vol. 0(0) 1–25

DOI: 10.1177/13694332241255747
journals.sagepub.com/home/ase
Sage

Xiaofeng Zhang and Harry Far

Abstract

In the traditional design method, structures are usually assumed as rigid base structures without considering soil-structure interaction (SSI). However, whether the effect of SSI on the seismic performance of structures is beneficial or detrimental is far from consensus among researchers. Moreover, previous literature mostly concentrated on the seismic behaviour of mid-rise buildings and moment-resisting frames. Therefore, it is in real need to comprehensively investigate the seismic response of tall buildings considering SSI. In this study, a soil-foundation-structure model developed in finite element software and verified by shaking table tests is used to critically explore the effects of SSI on high-rise buildings with a series of superstructure and substructure parameters. The beneficial and detrimental impacts of SSI are identified and discussed. Numerical simulation results indicate the rise in the stiffness of subsoil can dramatically amplify the base shear of structures. As the foundation rotation increases, inter-storey drifts are increased, and base shears are reduced. In general, SSI amplifies the inter-storey drifts showing detrimental effects of SSI. However, as for the base shear, SSI exerts detrimental effects on most piled foundation cases as well as classical compensated foundation structures resting on C_e soil, whereas, for compensated foundation structures resting on soil types D_e and E_e, effects of SSI are beneficial since the base shear is reduced. Moreover, regarding buildings with different structural systems and foundation types, minimum base shear ratios considering the SSI reduction effect are presented.

Keywords

high-rise buildings, soil-structure interaction, inter-storey drifts, base shear, finite element analysis, seismic response

Introduction

With the reduction of urban construction land and the rise of land price, high-rise buildings with multiple underground stories are becoming more and more popular than several years ago (Al Agha et al., 2021; Bryce et al., 2019; Segaline et al., 2022). Among the various structural forms of tall buildings, frame-core tube structures and frame-shear wall structures combine the advantages of flexible layout and high ductility of frame structures and the advantages of large stiffness and high bearing capacity of shear wall structures (Gao et al., 2005). In general, when resisting earthquake action, the shear wall (core tube) is the first line of defence, and the frame is the second line of defence, forming dual lateral force resistance systems to provide excellent abilities to resist earthquake effects (Lu, 2005; Son et al., 2017). As a result, frame-core tube structures and frame-shear wall structures with multiple basement stories are the most common structural forms of tall buildings in the world today (Ayala et al., 2022; Karki et al., 2021).

In the design process of tall buildings, the fixed-base assumption is only valid when the structure is constructed on a stiff soil medium because the foundation input motion is almost equal to the free-field motion (Far, 2020; Haydar et al., 2018; Saleh et al., 2018). If the structure is rested on relatively soft subsoil, the foundation input motion will not conform to the free-field motion due to the rigidity of the foundation (Anand and Satish Kumar, 2018; Far and Flint 2017; Lin et al., 2019). In addition, the seismic response of the structure

School of Civil and Environmental Engineering, Faculty of Engineering and Information Technology, University of Technology Sydney (UTS), Sydney, NSW, Australia

Corresponding author:
Xiaofeng Zhang, School of Civil and Environmental Engineering, Faculty of Engineering and Information Technology, University of Technology Sydney (UTS), Building 11, Level 11, Broadway, Ultimo, Sydney, NSW 2007 (PO Box 123), Australia.
Email: xiaofeng.zhang@student.uts.edu.au

may deform the subsoil and alter the input motion (Wolf and Deeks, 2004). These two impacts, normally referred to as kinematic interaction and inertial interaction, are the main mechanisms behind soil-structure interaction (SSI).

After the soil system is considered, a large part of the energy is dissipated into the subsoil when the superstructure is in vibration (Wolf, 1985) and the increased damping will considerably alleviate the seismic response and decrease the base shear (V). Nevertheless, horizontal movement and rotation of the foundation will be incorporated into the soil-structure system because of the flexibility and compatibility of the subsoil, which can increase the lateral deformations (Δ) and inter-storey drifts (δ) of the superstructure (Far, 2019; Tabatabaiefar and Clifton, 2016). Therefore, whether the effect of SSI is beneficial or detrimental needs to be further investigated and discussed.

In terms of commonly used governing parameters in seismic analyses (V, δ and Δ), the SSI effects in recent studies have been summarised in Table 1. It can be seen that how SSI affects structure is far from consensus among researchers. In addition, previous literature mostly concentrated on the seismic behaviour of mid-rise buildings and moment-resisting frames. Therefore, it is in real need to comprehensively investigate the seismic response of tall buildings considering SSI.

In this study, a numerical soil-structure model is established using *Abaqus* to investigate the seismic response of high-rise buildings. The shaking table tests were employed to verify the validity of the numerical model. After that, extensive parametric studies have been conducted on frame-core tube structures and frame-shear wall structures. The parameters include structural heights, height-width

Table 1. Summary of SSI Effects in Previous Studies.

References	Superstructure type	Foundation type	Effects of SSI
Galal and Naimi (2008)	6 and 20-storey reinforced concrete (RC) frames	Shallow foundation	$V\downarrow$, $\delta\uparrow$
Tabatabaiefar and Massumi (2010)	3, 5, 7 and 10-storey RC frames	Shallow foundation	$V\downarrow$, $\delta\uparrow$, $\Delta\uparrow$
Carbonari et al. (2011 and 2012)	6-Storey wall-frame structure	Piled foundation	$V_{wall}\downarrow$, $V_{frame}\uparrow$, $\delta\uparrow$, $\Delta\uparrow$
Tabatabaiefar et al. (2013)	10-Storey RC frame	Shallow foundation	$V\downarrow$, $\delta\uparrow$, $\Delta\uparrow$
Hokmabadi et al. (2014)	15-Storey RC frame	Shallow foundation and floating pile foundation	$V\downarrow$, $\delta\uparrow$, $\Delta\uparrow$
Tabatabaiefar and Fatahi (2014)	5, 10 and 15-storey RC frames	Shallow foundation	$\delta\uparrow$, $\Delta\uparrow$
Hokmabadi et al. (2015)	5, 10 and 15-storey RC frames	End-bearing pile foundation	$\delta\uparrow$, $\Delta\uparrow$
Karapetrou et al. (2015)	9-Storey RC frame	Shallow foundation	$V\downarrow$, $\delta\downarrow$, $\Delta\downarrow$
Yeganeh et al. (2015)	17-Storey RC frame	Shallow foundation	$V\downarrow$, $\delta\downarrow$
Van Nguyen et al. (2017)	15-Storey RC frame	Floating pile/end-bearing pile foundation	$V\uparrow$, $\delta\uparrow$
Ghandil and Behnamfar (2017)	5, 10, 15 and 30-storey steel frames	Shallow/piled foundation	$V\downarrow$, $\delta\uparrow$
Bagheri et al. (2018)	15 and 30-storey steel frames	Six types of piled raft foundations	$V\downarrow$, $\delta\uparrow$, $\Delta\uparrow$
Samanta and Swain (2019)	3, 6 and 9-storey RC frames	Piled foundation	$\Delta\uparrow$
Liu et al. (2020)	6-Storey steel frame	Piled foundation	$\delta\downarrow$, $\Delta\downarrow$
Qaftan et al. (2020)	15-Storey wall-frame structure	2 basement stories on piled foundation	$\Delta\uparrow$
Scarfone et al. (2020)	20-Storey wall-frame structure	Shallow/deeply embedded pile foundation	$V\downarrow$, $\delta\downarrow$, $\Delta\downarrow$
Yang et al. (2020)	12-Storey RC frame	Piled foundation	$V\downarrow$, $\delta\downarrow$, $\Delta\downarrow$
Fathi et al. (2020)	A historic masonry building	Brick and stone masonry	$\Delta\uparrow$
Arboleda-Monsalve et al. (2020)	40-Storey frame with and without shear wall	Shallow foundation	$\delta\uparrow$
Ansari et al. (2021)	12, 18, and 24-storey RC frames	Shallow and pile foundations	$V\downarrow$, $\delta\uparrow$
Nasab et al. (2021)	5-story soft first-story building	Shallow foundation	$\delta\uparrow$
Zhang et al. (2022)	20-Storey steel moment resist frame	Embedded box foundation	$\delta\uparrow$
Kamal et al. (2022)	5, 8, 10, 13, and 15-storey RC frames	Mat foundations	$\Delta\uparrow$
Wang and Yang (2022)	1∼15-storey RC frames	Pile foundation	$V\downarrow$or$\uparrow$, $\delta\downarrow$or$\uparrow$
Liang et al. (2023)	51-story frame core tube structure	Group pile foundation	$V\downarrow$, $\delta\uparrow$, $\Delta\uparrow$

Note: ↑ = this parameter increases after SSI is taken into account; ↓ = this parameter decreases after SSI is taken into account.

ratios (HWR), foundation types, soil types and bedrock depths (BD). For each case, four different seismic records were applied to investigate the seismic governing factors (V and δ) of the superstructure. Therefore, this study has calculated a total of 72 rigid base cases and 720 flexible base cases. By analysing the seismic response of a great number of tall buildings cases, the beneficial and detrimental scenarios for high-rise buildings considering SSI can be identified and code-based procedures are developed to provide a safe and economical structural design method.

Parameters of the structure and the subsoil

Two commonly used structural systems: frame-core tube structure and frame-shear wall structure with three different structural heights: 60 m (20-storey), 90 m (30-storey) and 120 m (40-storey) are considered in this study. For each structural height, three HWRs of 4, 5, six are considered. The arrangement of shear walls (core tube) and columns is shown in Figure 1(a) and Figure 2(a). According to AS 1170.4 (2007), three different soil types: C_e, D_e, and E_e soil are adopted and their geotechnical properties are presented in Table 2 (Tabatabaiefar and Fatahi, 2014). Additionally, as shown in Figure 1(b) and (c) and Figure 2(b) and 2(c), end bearing piled foundation and classical compensated foundation are taken into account. A compensated foundation in building design is sufficiently deep to allow the removed soil weight to offset the building weight. The arrangement and dimensions of piles for buildings of different heights and HWRs have shown in Figure 3 and Table 3. For each

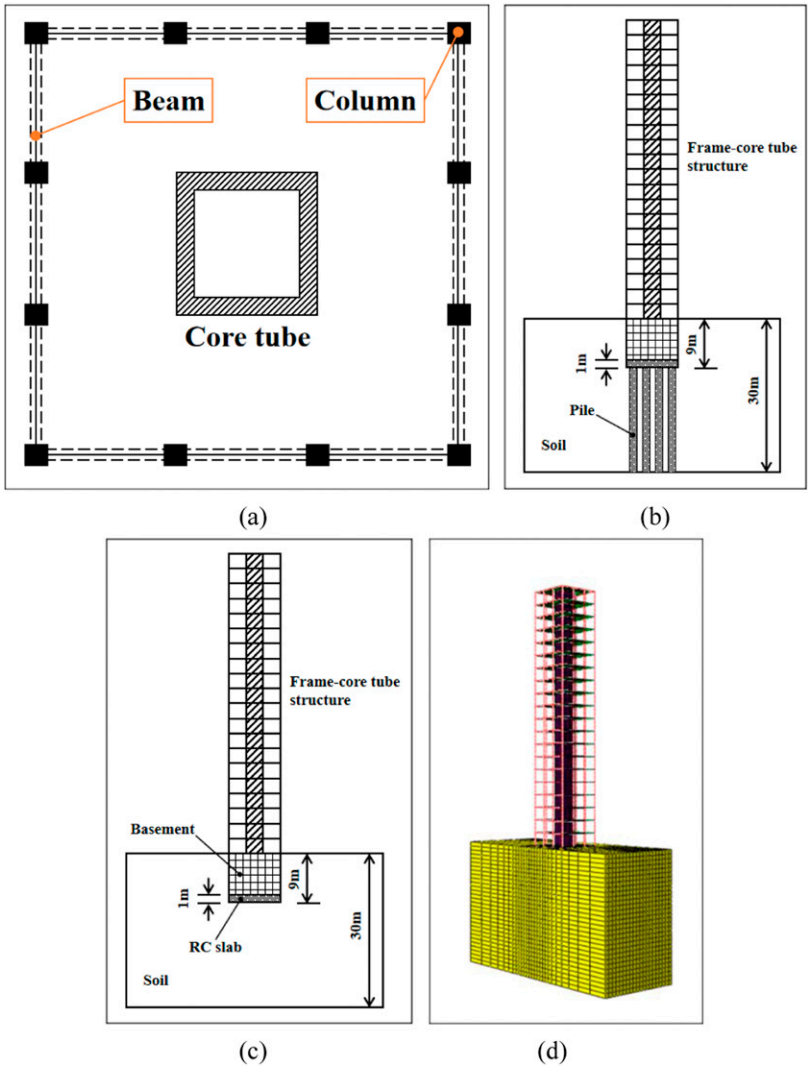

Figure 1. The setup of the frame-core tube structure: (a) plan view of the standard storey (b) end bearing piled foundation-supported structure (c) classical compensated foundation-supported structure (d) the finite-element model.

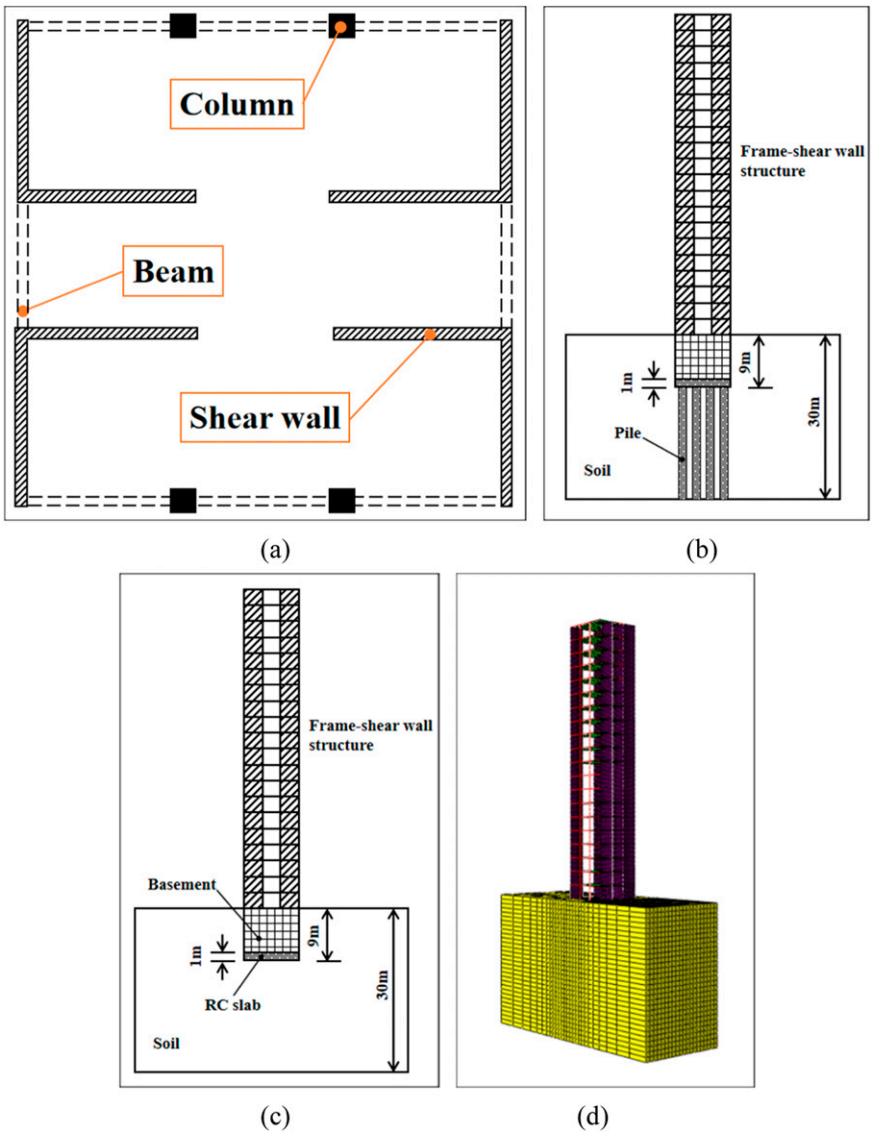

Figure 2. The setup of the frame-shear wall structure: (a) plan view of the standard storey (b) end bearing piled foundation-supported structure (c) classical compensated foundation-supported structure (d) the finite-element model.

Table 2. Geotechnical Characteristics of the Subsoil.

Soil type (AS1170)	Unified classification (USCS)	Shear wave velocity (V_s) (m/s)	G_{max} (kPa)	Soil density (kg/m^3)	Poisson's ratio	c' (kPa)	φ' (degree)	Plastic Index
C_e	GM	600	623,400	1730	0.28	5	40	-
D_e	CL	320	177,300	1730	0.39	20	19	20
E_e	CL	150	33,100	1470	0.40	20	12	15

model, two far-field and two near-field earthquake motions (Figure 4) are applied.

The structural sections are designed using SAP2000 V 20 software according to AS3600 (2018) and AS1170.4 (2007). The specified compressive strength, modulus of elasticity and unit weight of concrete are 40 MPa, 32.8 GPa and 24.5 kN/m^3, respectively. Nonlinear time-history analyses were then conducted under earthquakes records in Figure 4 to ensure the maximum inter-storey drifts of all rigid-base models are less than 1.5% according AS1170.4

(2007), Clause 5.5.4. The dimensions of shear walls, columns, beams and slabs of structures with different heights are shown in Table 4. In order to compare the results conveniently, the same component dimensions are adopted for the high-rise buildings with different HWRs. The natural periods of fixed-base and flexible-base models are given in Tables 5–10.

Numerical simulation procedure

Numerical model of the superstructure

Abaqus 6.14 software (Dassault Systèmes SIMULIA, 2012) is adopted to model the soil-structure system. To reduce the calculation time of a single model under the premise of ensuring accuracy, 4-node general-purpose shell elements with reduced integration are selected to simulate slabs and shear walls. Three dimensional 2-node linear beam elements are selected to simulate beams and columns. The basement, piles and soil domain are modelled by 8-node solid elements with reduced integration. Figure 1(d) and Figure 2(d) present the mesh of the finite element model. Moreover, elastic-perfectly plastic behaviour is adopted in superstructure elements. Because the superstructures in this study are all reinforced concrete structures, the damping ratio is taken as 5%.

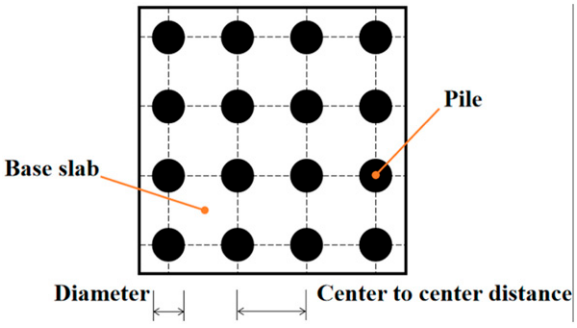

Figure 3. Pile arrangement adopted in this study.

Numerical model of the subsoil

Rayhani and Naggar (2008) suggests the horizontal dimension of the soil domain should be at least five times the width of the superstructure. Because the superstructure height and HWR adopted in this study are variable, the width of the superstructure is also variable (from 10 m to 30 m). Therefore, the horizontal dimensions of the soil domain vary between 50 m and 150 m (five times the width of the superstructure). Moreover, as shown in Figures 1 and 2, the bedrock depth is assumed to be 30 m since the most amplification effects occur within the top 30 m of the subsoil (Rayhani and Naggar, 2008).

When meshing the ground soil, the guideline proposed by Gazetas (1983) is employed. The height of the soil element should be (1/5∼1/8) versus/f_{max}, where f_{max} is the highest wave frequency considered. In this study, seismic records are filtered to prevent frequencies higher than 25 Hz so as to limit the dimension of soil elements without affecting the accuracy of results.

To accommodate the nonlinearity of the subsoil, the approach adopted involved the utilisation of cyclic shear strain-dependent shear modulus curves (Figure 5) and damping ratio curves (Figure 6). These curves were integrated into the analysis to better capture the intricate response of the subsoil under seismic loading conditions. The determination of strain-compatible values for soil damping and shear modulus under different seismic records necessitated the application of a trial and error methodology. This method involved the systematic adjustment of these parameters until a satisfactory alignment between predicted and observed responses was attained for each seismic event. For a comprehensive understanding of this approach, reference is directed to the detailed procedures delineated in the works of Tabatabaiefar et al. (2013) and Fatahi and Tabatabaiefar (2014). These seminal contributions offer thorough insights into the theoretical framework and practical implementation of the proposed methodology, elucidating the steps involved in calibrating soil properties to accurately reflect the observed nonlinear behaviour.

Table 3. Configuration of Piles of Structures With Different Heights and HWRs

Structures	HWRs	Diameter (m)	Centre to centre distance (m)
20-Storey	4	1.2	4
	5	1.2	3
	6	1.2	2.6
30-Storey	4	1.5	6
	5	1.5	5
	6	1.5	4
40-Storey	4	2	8
	5	2	6
	6	2	5

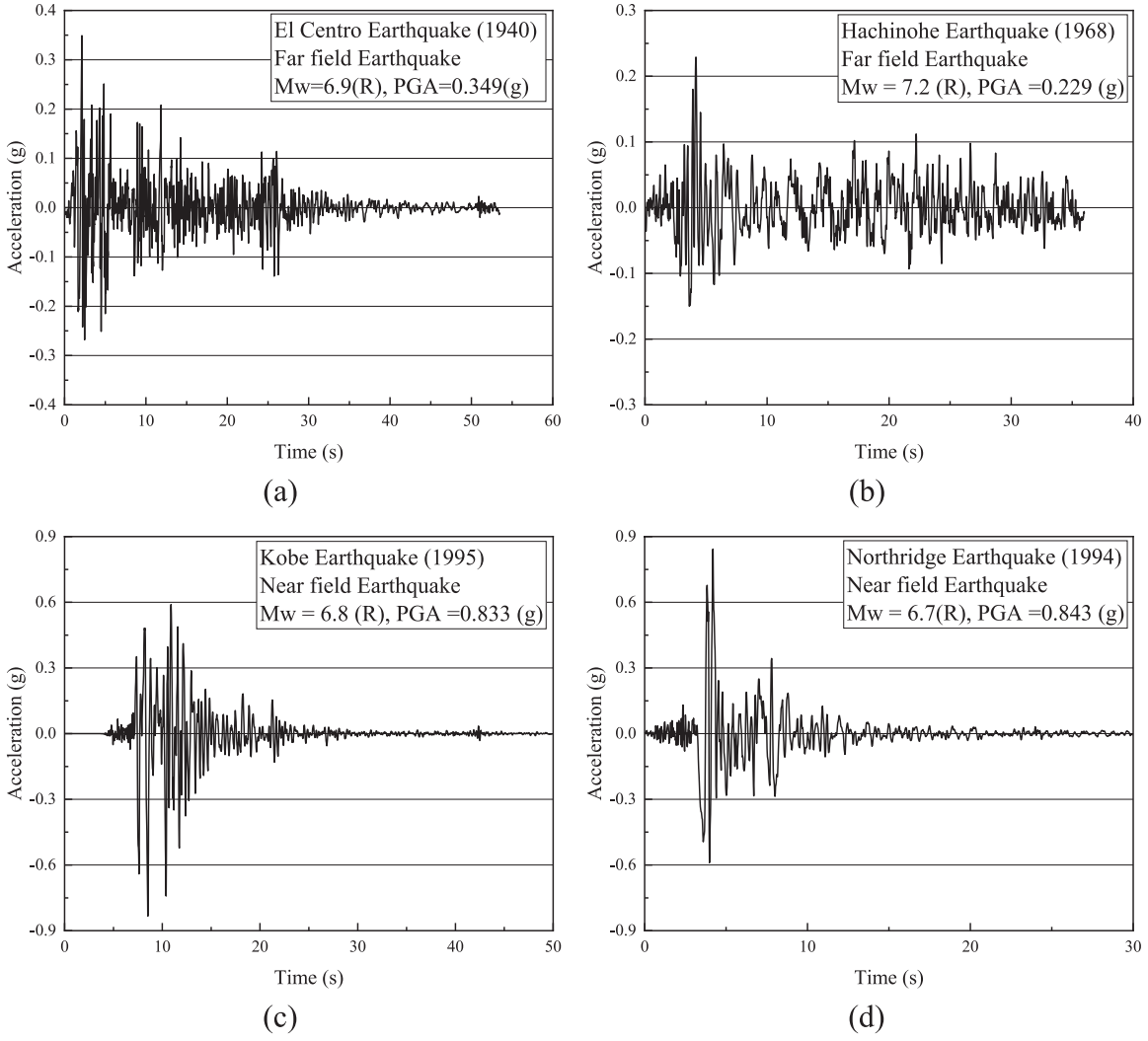

Figure 4. Adopted seismic records: (a) El Centro earthquake; (b) Hachinohe earthquake; (c) Kobe earthquake; (d) Northridge earthquake.

Table 4. Dimensions for Sections of Studied Models (m).

Structures	Storey level	Shear walls	Columns	Beams	Slabs
20-Storey	1~5	0.55	0.55×0.55	0.40×0.40	0.25
	6~10	0.50	0.50×0.50	0.40×0.40	0.25
	11~15	0.45	0.45×0.45	0.40×0.40	0.25
	16~20	0.40	0.40×0.40	0.40×0.40	0.25
30-Storey	1~10	0.70	0.70×0.70	0.50×0.50	0.25
	11~20	0.60	0.60×0.60	0.50×0.50	0.25
	21~30	0.50	0.50×0.50	0.50×0.50	0.25
40-Storey	1~10	0.80	1.00×1.00	0.50×0.80	0.25
	11~20	0.70	0.90×0.90	0.50×0.80	0.25
	21~30	0.60	0.80×0.80	0.50×0.80	0.25
	31~40	0.50	0.70×0.70	0.50×0.80	0.25

Table 5. Natural Periods of 20-Storey Fixed-base and Flexible-base Frame-core Tube Models (s).

		Flexible-base model					
		Piled foundation			Classical compensated foundation		
HWR	Fixed-base model	E_e soil	D_e soil	C_e soil	E_e soil	D_e soil	C_e soil
6	1.203	1.461	1.312	1.273	1.736	1.387	1.325
5	1.165	1.456	1.309	1.277	1.626	1.376	1.322
4	1.128	1.411	1.294	1.238	1.586	1.355	1.269

Table 6. Natural Periods of 30-Storey Fixed-base and Flexible-base Frame-core Tube Models (s).

		Flexible-base model					
		Piled foundation			Classical compensated foundation		
HWR	Fixed-base model	E_e soil	D_e soil	C_e soil	E_e soil	D_e soil	C_e soil
6	2.004	2.447	2.167	2.093	2.767	2.208	2.105
5	1.941	2.354	2.158	2.068	2.742	2.246	2.115
4	1.870	2.319	2.070	1.998	2.588	2.239	2.059

Table 7. Natural Periods of 40-Storey Fixed-base and Flexible-base Frame-core Tube Models (s).

		Flexible-base model					
		Piled foundation			Classical compensated foundation		
HWR	Fixed-base model	E_e soil	D_e soil	C_e soil	E_e soil	D_e soil	C_e soil
6	2.663	3.814	2.956	2.795	4.292	3.056	2.892
5	2.626	3.628	2.947	2.803	4.178	3.011	2.902
4	2.582	3.569	2.822	2.716	3.791	2.930	2.755

Table 8. Natural Periods of 20-Storey Fixed-base and Flexible-base Frame-Shear Wall Models (s).

		Flexible-base model					
		Piled foundation			Classical compensated foundation		
HWR	Fixed-base model	E_e soil	D_e soil	C_e soil	E_e soil	D_e soil	C_e soil
6	0.999	1.410	1.180	1.135	1.743	1.225	1.136
5	1.027	1.408	1.200	1.138	1.618	1.214	1.135
4	1.005	1.352	1.183	1.132	1.584	1.206	1.121

Table 9. Natural Periods of 30-Storey Fixed-base and Flexible-base Frame-Shear Wall Models (s).

		Flexible-base model					
		Piled foundation			Classical compensated foundation		
HWR	Fixed-base model	E_e soil	D_e soil	C_e soil	E_e soil	D_e soil	C_e soil
6	1.752	2.322	2.017	1.923	2.737	2.065	1.931
5	1.798	2.264	2.016	1.935	2.717	2.068	1.943
4	1.768	2.236	1.989	1.917	2.593	2.028	1.923

Table 10. Natural Periods of 40-Storey Fixed-base and Flexible-base Frame-Shear Wall Models (s).

		Flexible-base model					
		Piled foundation			Classical compensated foundation		
HWR	Fixed-base model	E_e soil	D_e soil	C_e soil	E_e soil	D_e soil	C_e soil
6	2.450	3.252	2.873	2.679	3.773	2.826	2.641
5	2.482	3.195	2.875	2.692	3.756	2.867	2.701
4	2.512	3.281	2.853	2.683	3.375	2.857	2.685

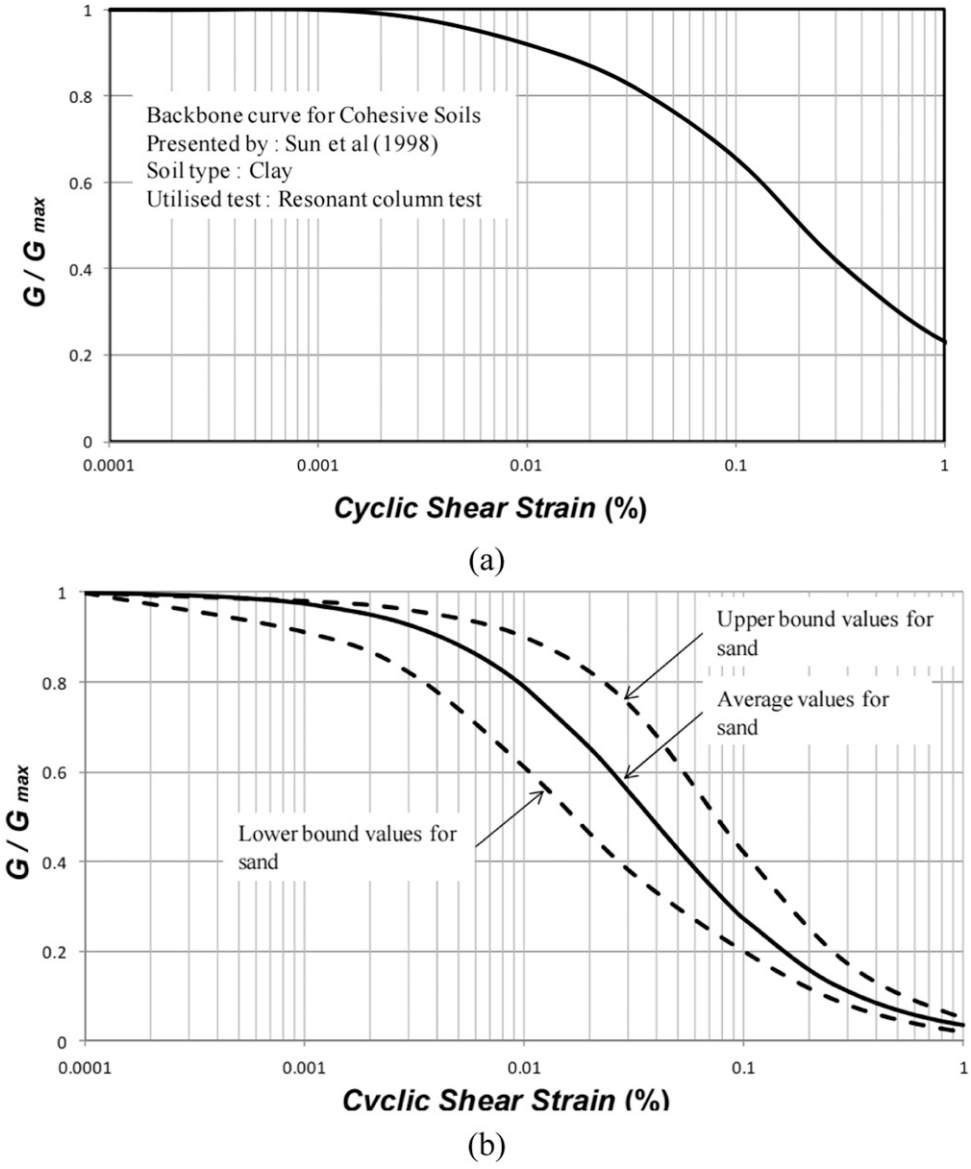

Figure 5. Shear modulus reduction curves: (a) cohesive soil (after Sun et al., 1998); (b) cohesionless soil (after Seed et al., 1986).

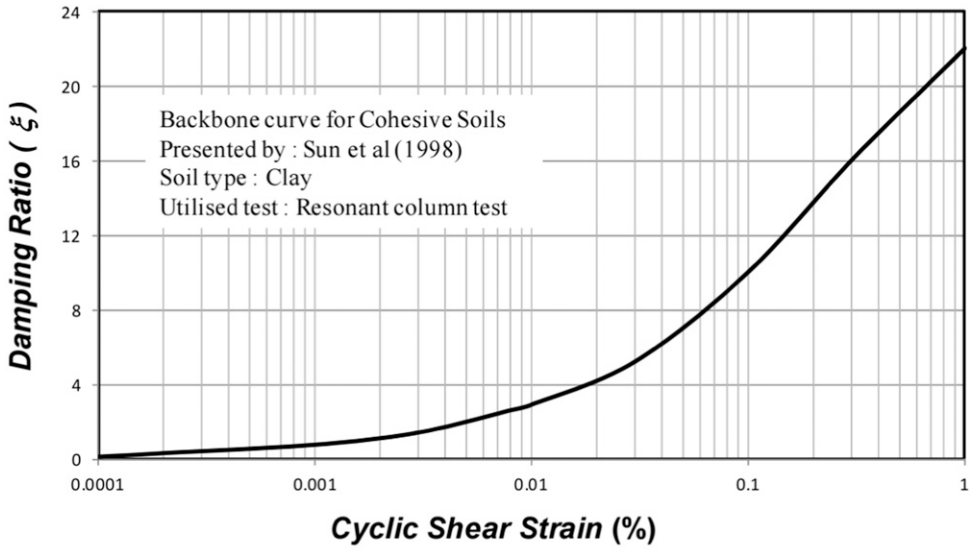

(a)

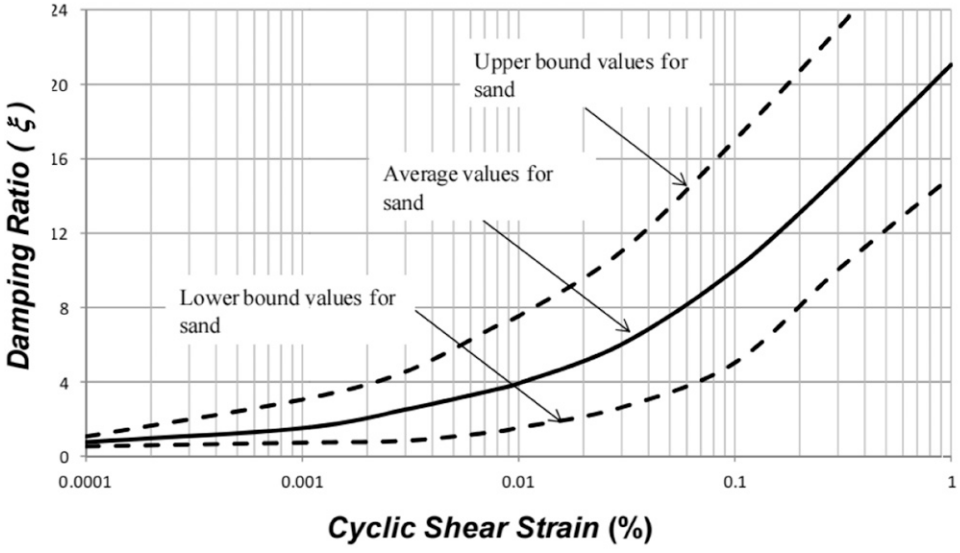

(b)

Figure 6. Damping curves: (a) cohesive soil (after Sun et al., 1998); (b) cohesionless soil (after Seed et al., 1986).

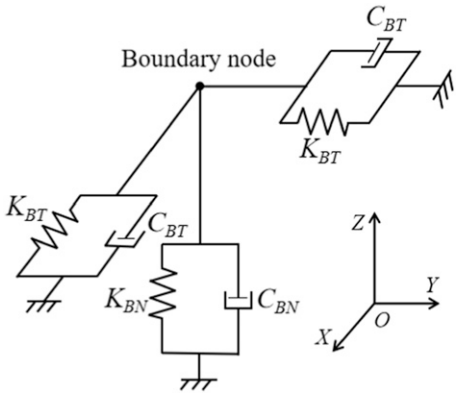

Figure 7. Viscous-spring boundary.

Rayleigh damping is adopted to take into account the energy loss in the subsoil in an earthquake event. When calculating damping coefficients, two soil-structure model frequencies covering the range with a significant amount of input motion are adopted (Park and Hashash, 2004).

Boundary conditions

In this study, viscous-spring boundary was applied on lateral and bottom surfaces of the subsoil domain to avoid the reflection of outward propagating waves, independent springs and dampers in three directions are specified on the boundary nodes (Figure 7). The coefficients of the springs

(K_T and K_N) and dampers (C_T and C_N) can be obtained as follows (Gu et al., 2007):

$$K_T = \alpha_T\, G/R, C_T = \rho\, V_S \tag{1}$$

$$K_N = \alpha_N\, G/R, C_N = \rho\, V_P \tag{2}$$

Where α_T, α_N are modified coefficients, and their values are suggested by Liu et al. (2006). Subscripts T and N indicate tangential and normal directions. R is the distance between the wave source and boundary nodes; ρ, G and V_p are the density, shear modulus and P wave velocity of the ground soil, respectively.

Figure 8. Completed fixed-base model of shaking table tests (Tabatabaiefar and Mansoury, 2016; Zhang and Far, 2022).

Input of earthquake motions

During dynamic time-history analyses, the motion of boundary nodes is supposed to conform to the free-field motion to supply conditions identical to the infinite model. To achieve this goal, the equivalent node force method is adopted. In this method, first of all, the free-field strain of the boundary is obtained from the geometric equation, and then the stress on the boundary is obtained by stress-strain relationship. After that, the boundary node balance relationship is used to calculate the equivalent earthquake load on the boundary node, that is, the equivalent node force ($\boldsymbol{F_b}$). Next $\boldsymbol{F_b}$ is applied on boundary nodes of the soil domain in the form of concentrated forces to realize the seismic wave input.

$\boldsymbol{F_b}$ consists of three terms: the first two terms are employed to compensate for the impacts of springs and dashpots on the boundary nodes, and the third term is the free field stress on the boundary (Ma et al., 2020):

$$\boldsymbol{F_b} = \left(\boldsymbol{K_b}\boldsymbol{u_b^{ff}} + \boldsymbol{C_b}\boldsymbol{v_b^{ff}} + \boldsymbol{\sigma_b^{ff}}\boldsymbol{n}\right)\boldsymbol{A_b} \tag{3}$$

Where $\boldsymbol{u_b^{ff}}$ and $\boldsymbol{v_b^{ff}}$ are free-field displacement vectors and velocity vectors; $\boldsymbol{K_b}$ and $\boldsymbol{C_b}$ are springs and dashpots

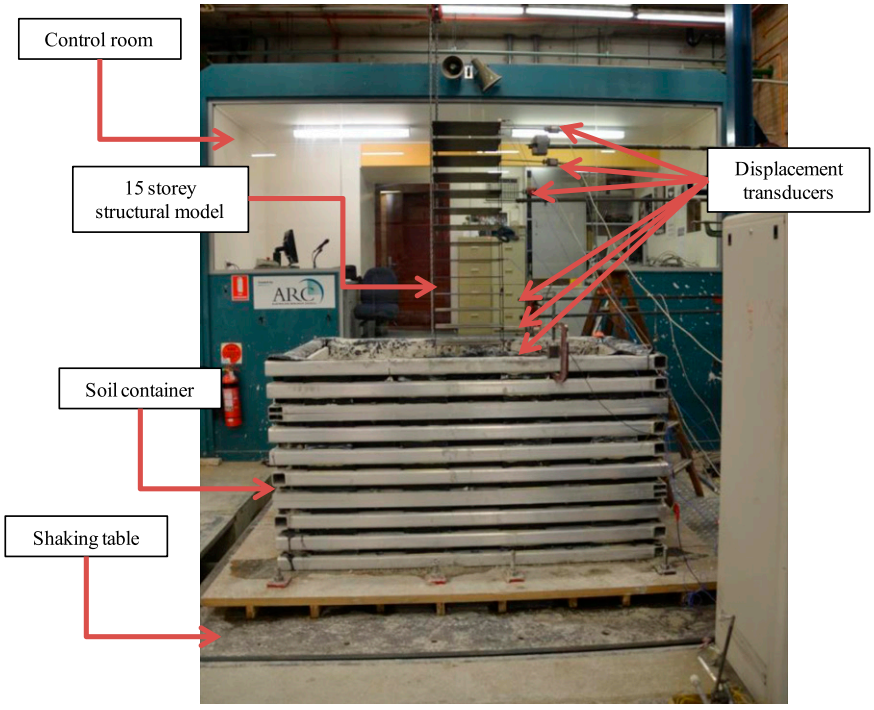

Figure 9. Completed soil-structure model of shaking table tests (Tabatabaiefar and Mansoury, 2016; Zhang and Far, 2022).

coefficient vectors. A_b is the influencing area of boundary nodes and $\boldsymbol{n}$ is the cosine vector of the normal direction outside the boundary. $\boldsymbol{\sigma_b^{ff}}$ is the free-field stress tensor which can be derived from the geometric equation and linear elastic material stress-strain relationship.

According to the seismic motion input approach described above, a MATLAB program was compiled by the authors to calculate the amplitudes of $\boldsymbol{F_b}$, and then $\boldsymbol{F_b}$ was applied in three directions of each boundary node.

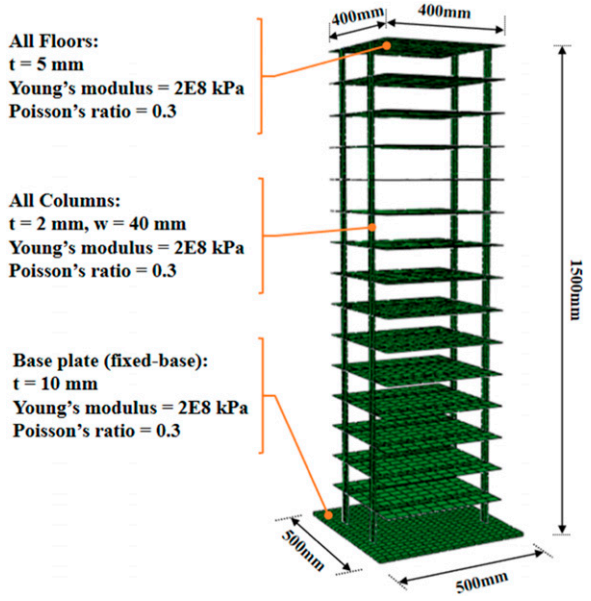

Figure 10. Fixed-base numerical model in *Abaqus*.

Verification of the numerical simulation method

To examine the accuracy of the adopted numerical modelling technique, shaking table tests were conducted on a 15-storey frame structure, and the results of numerical simulation were compared with the experimental results.

The fundamental frequency and mass of the prototype structure are 0.384 Hz and 953 tonnes respectively, and the structure is assumed to be built on clayey soil. In the scaling process, the objective is to achieve "dynamic similarity", in which same or similar accelerations and density of shaking table test model and prototype are desired (Meymand, 1998). After determining the scaling condition of the acceleration and density, the scaling relations for other variables, such as mass, time, length, etc., can also be derived and expressed in terms of geometric scaling factor (λ). By comparing specifications of the shaking table and characteristics of scaled models with different λ, λ of 1:30 is adopted. Therefore, the dimensions of the scaled structural model can be easily calculated to achieve geometric similarity. Moreover, the fundamental frequency and mass of the scaled model are determined to be 2.11 Hz and 106 kg respectively to achieve the dynamic similarity.

The mass of the assembled structure (Figure 8) is 104 kg and the fundamental frequency is 2.19 Hz, which are very close to the calculated value above. The scaled soil-

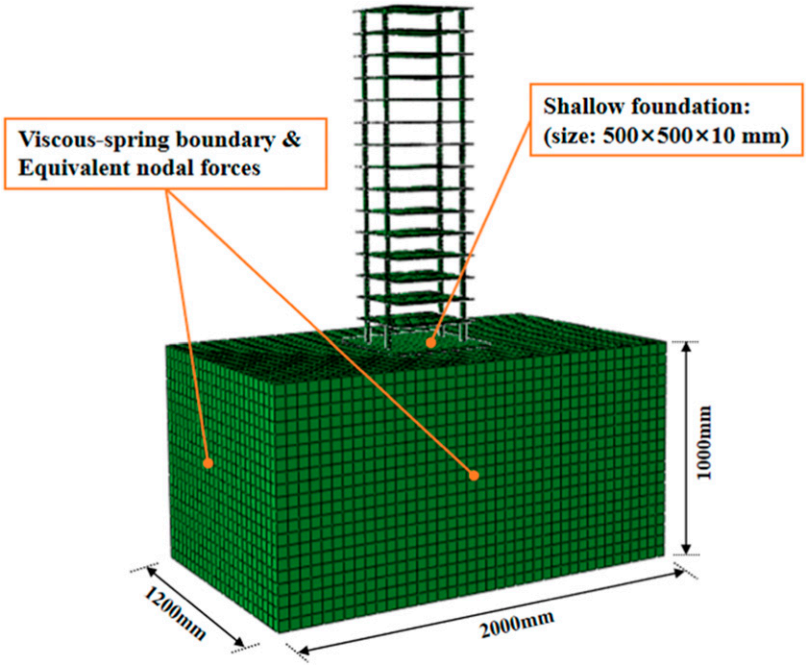

Figure 11. Flexible-base numerical model in *Abaqus*.

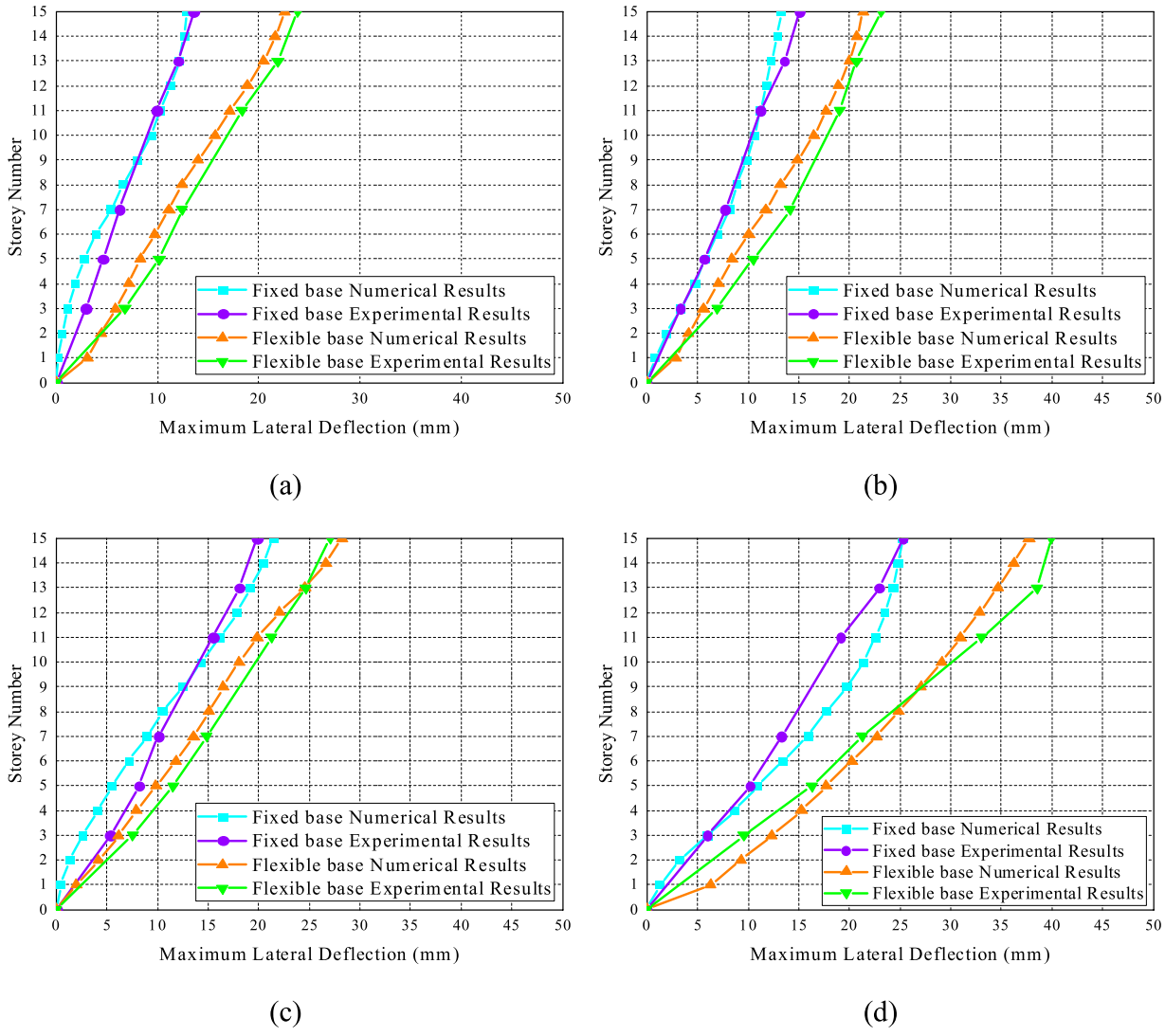

Figure 12. Numerical and experimental maximum lateral deflections of fixed-base and flexible-base models under the scaled (a) El Centro earthquake (b) Hachinohe earthquake (c) Kobe earthquake (d) Northridge earthquake.

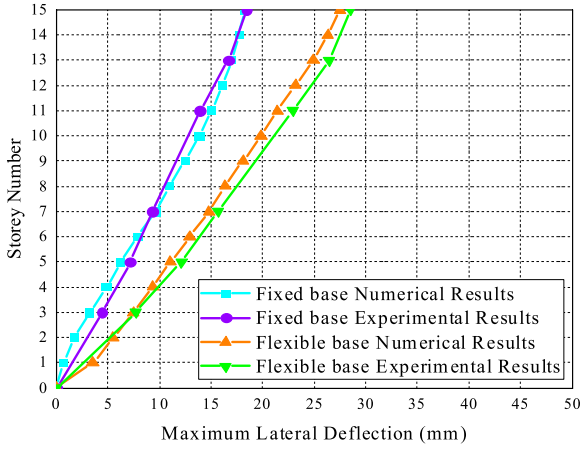

Figure 13. Average values of maximum lateral deflections of numerical and experimental models.

structure model is shown in Figure 9. More details about the shaking table tests can be found in Tabatabaiefar et al. (2014a), Fatahi et al. (2015), Tabatabaiefar and Mansoury (2016) and Tabatabaiefar (2016).

The identical numerical models (Figures 10 and 11) were also established in *Abaqus* software using the modelling technique described earlier. After that, numerical time-history analyses and shaking table tests were conducted under the action of four seismic records. The results in terms of the Δ of frame structure obtained from these two approaches are compared in Figures 12 and 13.

As shown in Figure 12, by comparing the values and trends of numerical calculations and experimental results, it can be drawn that the numerical model proposed in Section 3 is accurate enough to capture the seismic behaviour of buildings. Figure 13 indicates that errors of average Δ of

fixed-base and flexible-base models are only 8.8% and 5.6%, respectively. Therefore, the numerical simulation technique developed in this study is a rational and appropriate tool for SSI analyses.

Results and discussions

To compare the effects of different parameters more intuitively, the results determined from numerical soil-structure models including base shears (V_{fle}) and maximum inter-storey drifts (δ_{fle}) are normalised by those obtained from conventional fixed-base models (V_{fix} and δ_{fix}). As a result, if the value of the base shear ratio (V_{fle}/V_{fix}) or inter-storey drifts ratio ($\delta_{fle}/\delta_{fix}$) is greater than 1, it means that the SSI amplifies the V or δ and thus, its effect is detrimental. In addition, values of V_{fle}/V_{fix} and $\delta_{fle}/\delta_{fix}$ under the action of four seismic records (Figure 4) are averaged in this study so as to analyse and compare the data comprehensively and clearly demonstrate the impacts of superstructure and substructure parameters on high-rise buildings.

Effects of parameters on frame-core tube structures

Firstly, the value of V_{fle}/V_{fix} with different superstructure and substructure parameters are shown in Figures 14–19. It

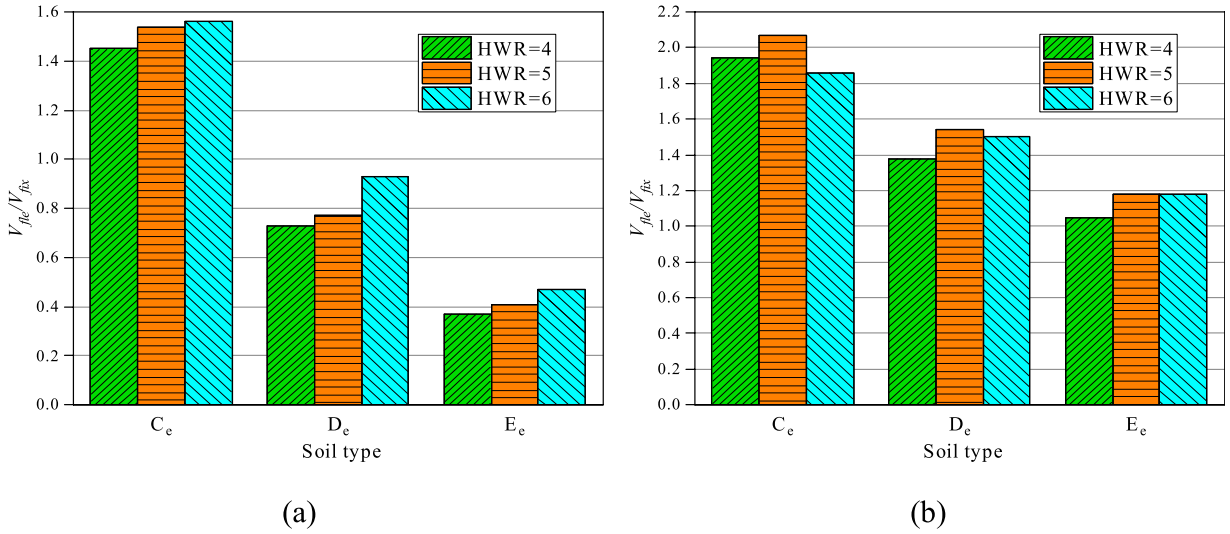

Figure 14. The value of V_{fle}/V_{fix} of 20-storey frame-core tube structures with different HWRs (a) classical compensated foundation structure (b) piled foundation structure.

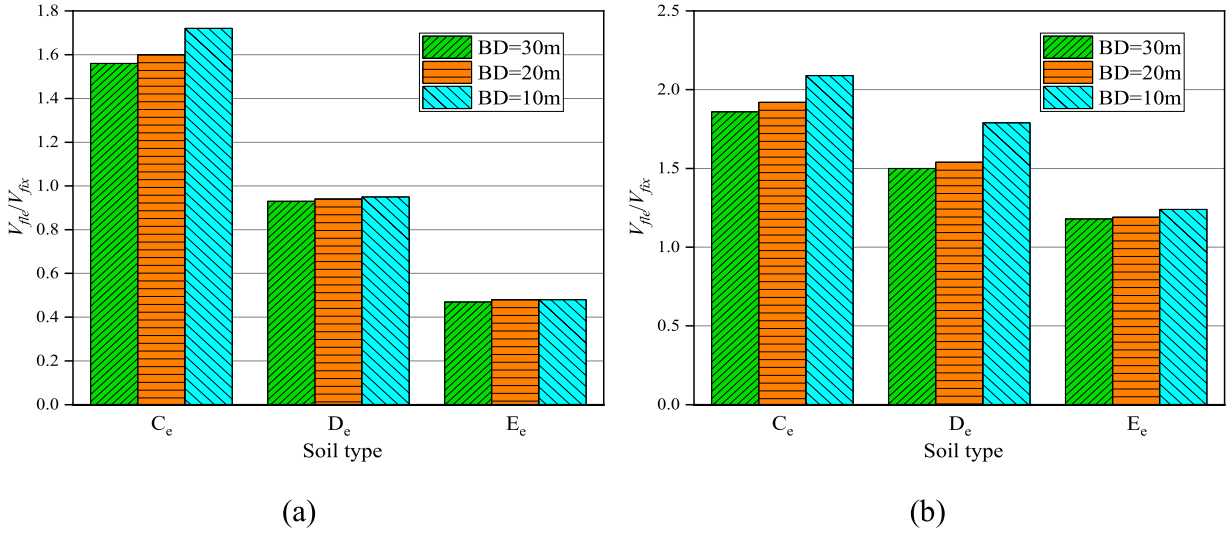

Figure 15. The value of V_{fle}/V_{fix} of 20-storey frame-core tube structures with different BDs (a) classical compensated foundation structure (b) piled foundation structure.

can be found that regardless of the foundation type, V_{fle}/V_{fix} increase significantly with the increase of the soil stiffness. The change of HWR and BD can also slightly change this ratio, but its influence is far less than that of the soil type. For the classical compensated foundation structures, the values of V_{fle}/V_{fix} of structures with the C_e soil are always greater than 1, indicating that the stiff soil can increase the V of frame-core tube structures when SSI is considered. In contrast, V_{fle}/V_{fix} of structures built on D_e and E_e soil types are both less than 1, indicating that the V can be reduced when structures are built on medium or soft soils. After meticulous consideration of soil and foundation effects, it becomes apparent that not only does the natural period of the structure undergo alteration, but also, due to soil amplification and the ramifications of kinematic and inertial interaction, the response spectrum of the foundation input motion undergoes modifications compared to free field motion. Consequently, the base shear experienced by a structure founded on stiff soil may exceed that of a fixed base structure, disregarding SSI effects.

When it comes to piled foundation structures, more seismic energy can be absorbed during an earthquake event (Van Nguyen et al., 2017). This is because piled foundation structures are generally stiffer, and their natural periods are typically shorter than those of compensated foundation structure. Therefore, in the descending

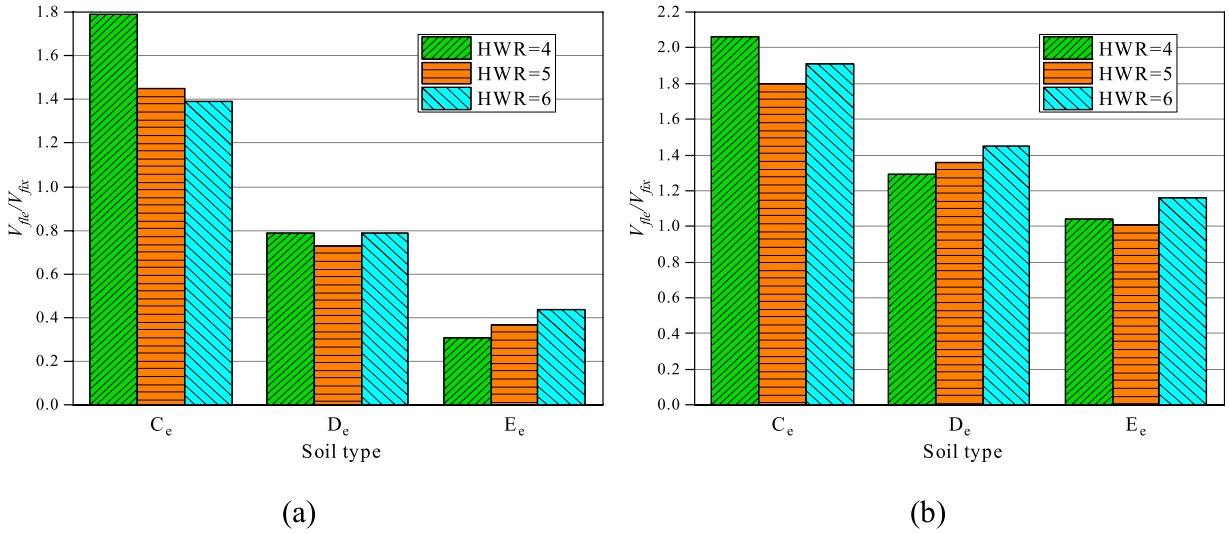

Figure 16. The value of V_{fle}/V_{fix} of 30-storey frame-core tube structures with different HWRs (a) classical compensated foundation structure (b) piled foundation structure.

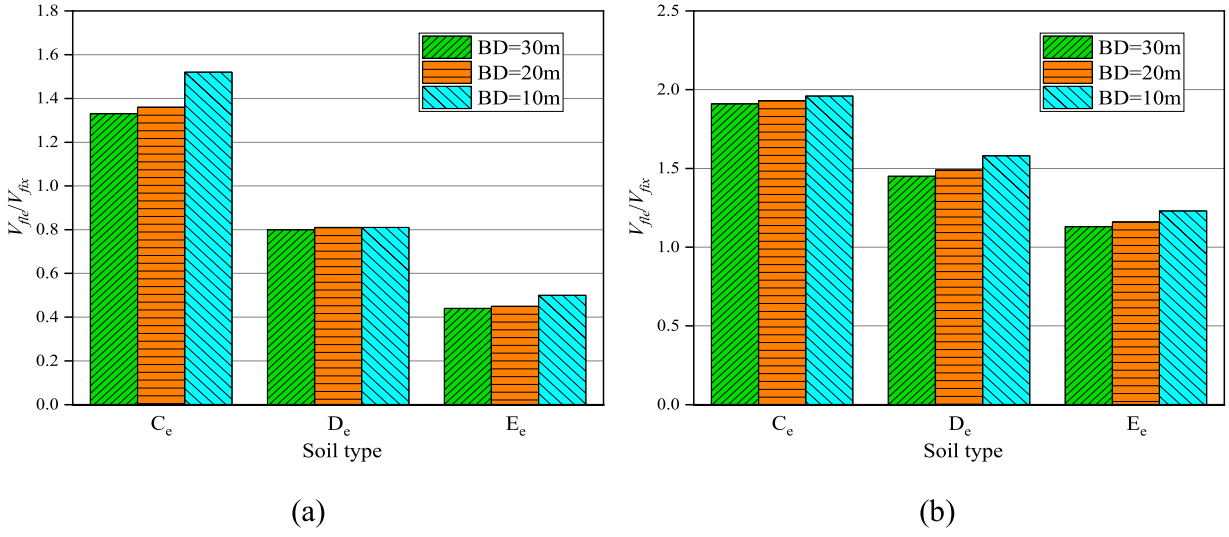

Figure 17. The value of V_{fle}/V_{fix} of 30-storey frame-core tube structures with different BDs (a) classical compensated foundation structure (b) piled foundation structure.

portion of the response spectrum, a shorter period implies higher seismic energy input. Moreover, due to soil amplification and the effects of kinematic and inertial interaction, the response spectrum of the foundation input motion also changes compared with free field motion. As a result, the values of V_{fle}/V_{fix} are greater than one in almost all piled foundation cases, which suggests that under the parameters considered here, the seismic demand of frame-core tube structures founded on the piled foundation is amplified after considering SSI. Therefore, for piled foundation structures, the effects of SSI are detrimental in terms of V.

Figures 20–25 show SSI always increases the δ because $\delta_{fle}/\delta_{fix}$ is greater than one in almost all cases. Therefore, SSI can alter the performance level of high-rise frame-core tube buildings. In addition, when superstructure and substructure parameters are changed, the influence of SSI on $\delta_{fle}/\delta_{fix}$ shows different trends. This is because the stiffness of the substructure has a complex effect on the deformation of the superstructure. On the one hand, as mentioned above, the increased stiffness of the substructure system can attract more seismic energy to deform the superstructure; on the other hand, stiffer ground soil can limit the foundation rocking, thereby reducing the deformation of

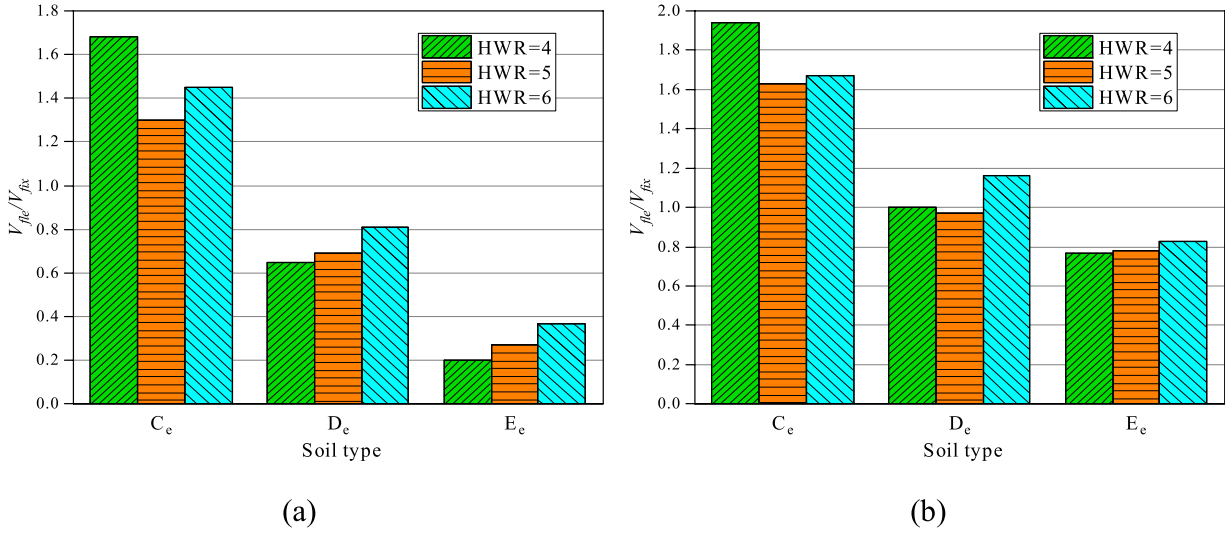

Figure 18. The value of V_{fle}/V_{fix} of 40-storey frame-core tube structures with different HWRs (a) classical compensated foundation structure (b) piled foundation structure.

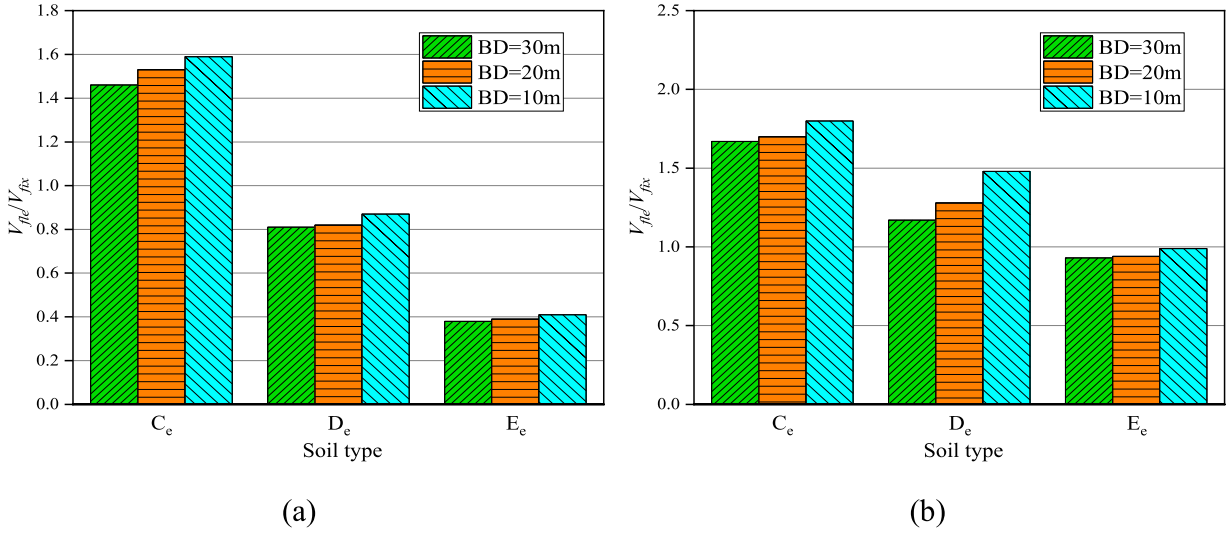

Figure 19. The value of V_{fle}/V_{fix} of 40-storey frame-core tube structures with different BDs (a) classical compensated foundation structure (b) piled foundation structure.

the superstructure. Thus, the V, δ and foundation rocking should be considered comprehensively.

According to Wolf (1985) and Kramer (1996), Δ consists of rocking (Δ_θ) and distortion components (Δ_d). In this study, proportions of lateral deflection caused by foundation rocking (Δ_θ/Δ) are adopted to reflect the significance of the foundation rocking under seismic events. In order to obtain this value under different parameters, firstly, the moment when the Δ occurred is recorded (Hokmabadi et al., 2012). After that, the Δ_θ is calculated by multiplying the height of the structure by the foundation rocking angle at this moment. Finally, the ratio Δ_θ/Δ can be calculated.

Figure 26 illustrates the relationship between $\delta_{fle}/\delta_{fix}$, V_{fle}/V_{fix} and Δ_θ/Δ of models with different superstructure and substructure parameters. When the subsoil is stiff enough and the values of Δ_θ/Δ are small (less than 0.5 for classical compensated foundation structures and less than 0.15 for piled foundation structures), the data points are basically distributed around the $y=x$ line. It indicates that the amplification coefficient for the V is almost equal to the amplification coefficient for the δ after considering SSI. Nevertheless, as soil stiffness decreases and the values of Δ_θ/Δ become larger, the data points begin to deviate from the $y=x$ line and shift downward to the right, indicating that the increase of the value of Δ_θ/Δ tends to

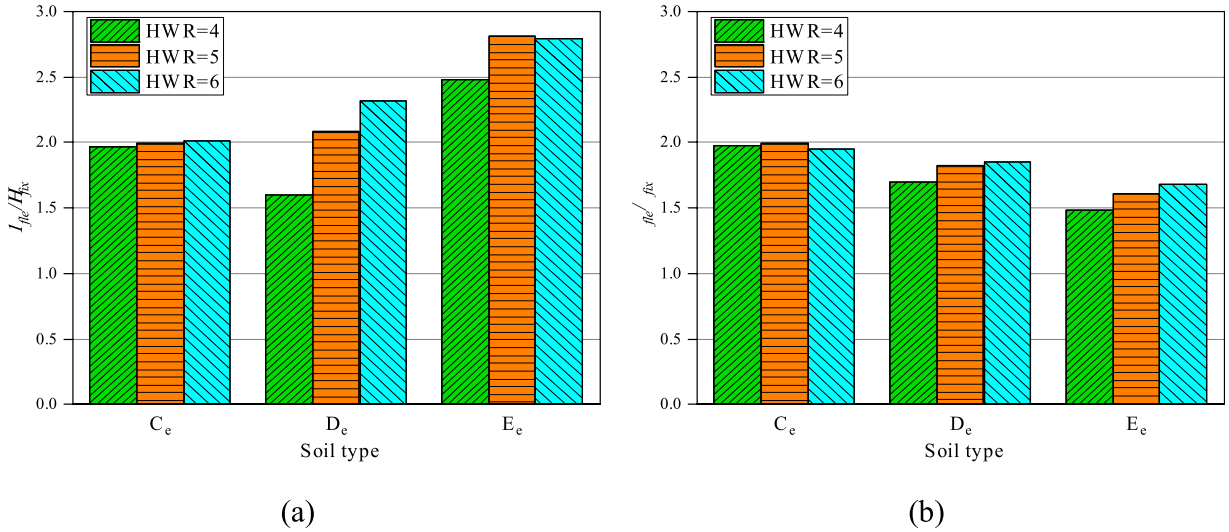

Figure 20. The value of $\delta_{fle}/\delta_{fix}$ of 20-storey frame-core tube structures with different HWRs (a) classical compensated foundation structure (b) piled foundation structure.

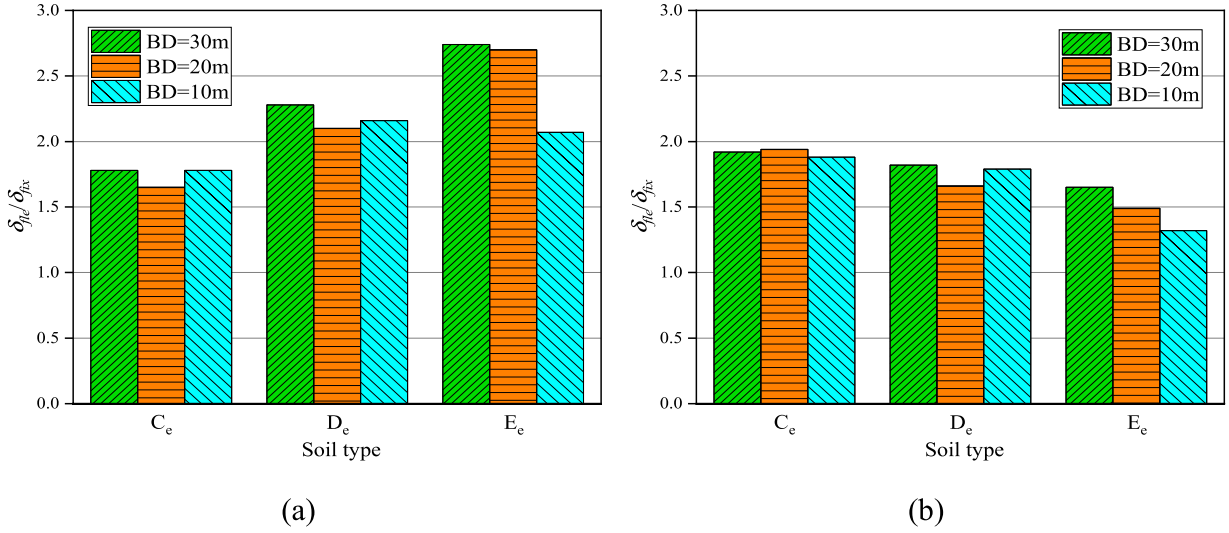

Figure 21. The value of $\delta_{fle}/\delta_{fix}$ of 20-storey frame-core tube structures with different BDs (a) classical compensated foundation structure (b) piled foundation structure.

amplify the δ and reduce the V of frame-core tube structures.

In addition, Figure 26 also reveals that almost all data points of the pile foundation model lie in the range of $\delta_{fle}/\delta_{fix} > 1$, $V_{fle}/V_{fix} > 1$, indicating that no matter how the model parameters change, the SSI has detrimental effects; however, for the classical compensated foundation model, structures with D_e and E_e soil types are below the $V_{fle}/V_{fix}=1$ line, indicating that the SSI has a beneficial effect, it can reduce the V of the superstructure, even if the δ are still amplified.

From the above analysis, SSI has detrimental effects on δ, and its effect on V is determined by foundation type and subsoil stiffness. However, as mentioned in the introduction section, previous studies are mainly focusing on the amplification of δ and neglecting the impact of SSI on the V, because most previous papers concluded SSI can reduce the V of the superstructure. For example, Tabatabaiefar et al. (2014b) developed an empirical formula to predict the value of $\delta_{fle}/\delta_{fix}$ and assess the performance level of buildings. Similarly, this study will summarise the effects of SSI on the V and develop a simple and accurate procedure to estimate the value of V_{fle}/V_{fix}.

Figure 27 shows the relationship between T_{fle}/T_{fix} and V_{fle}/V_{fix}. T is the natural period of vibration of the system. With the substructure stiffness decreasing and the T_{fle}/T_{fix}

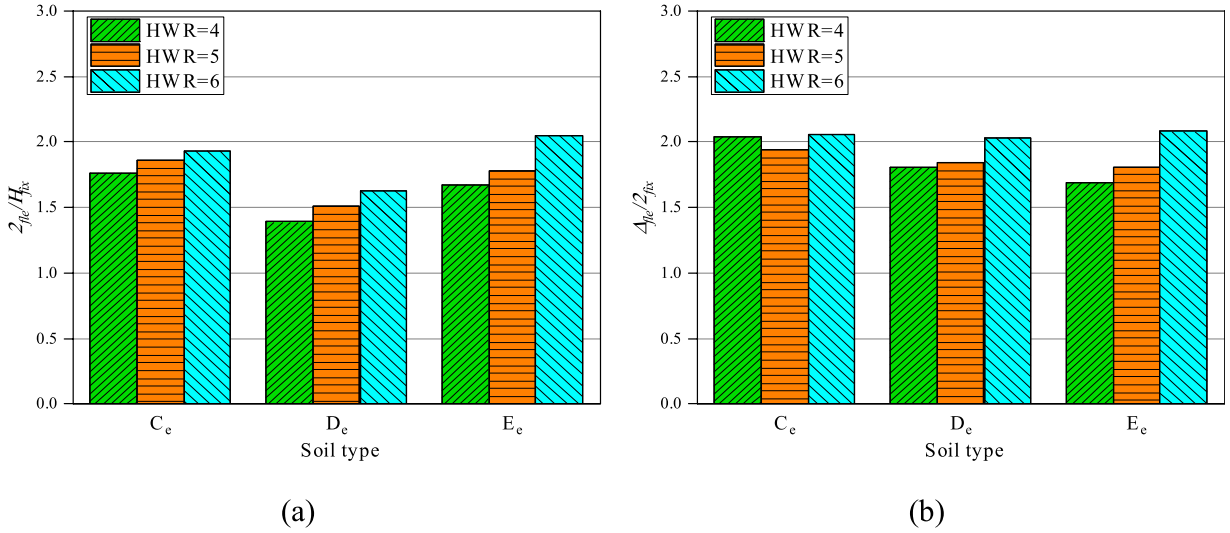

Figure 22. The value of $\delta_{fle}/\delta_{fix}$ of 30-storey frame-core tube structures with different HWRs (a) classical compensated foundation structure (b) piled foundation structure.

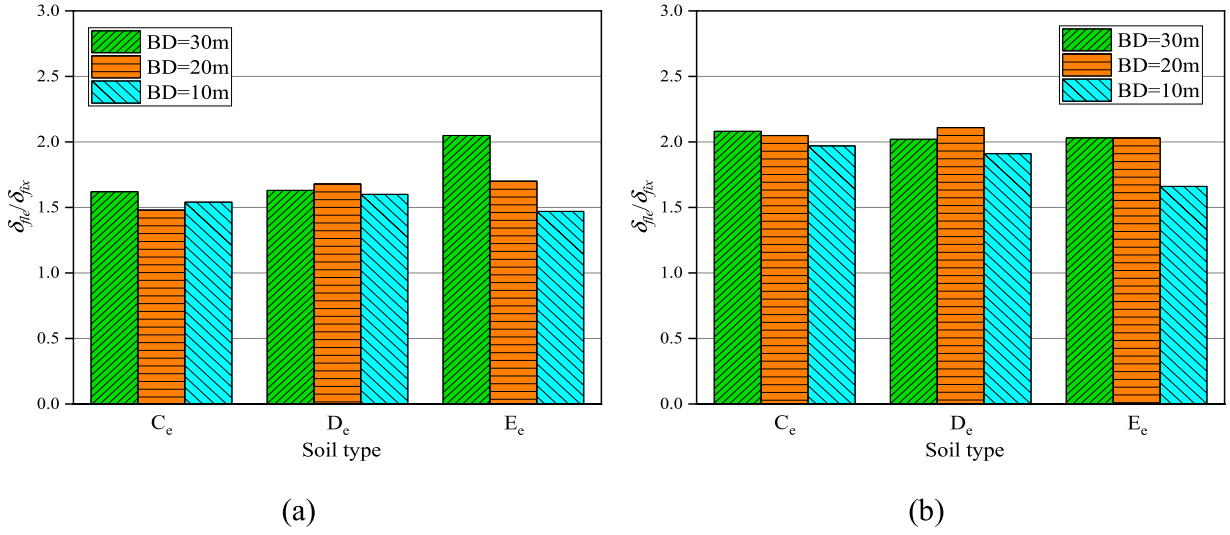

Figure 23. The value of $\delta_{fle}/\delta_{fix}$ of 30-storey frame-core tube structures with different BDs (a) classical compensated foundation structure (b) piled foundation structure.

increasing, V_{fle}/V_{fix} decreases linearly. But after reaching a certain level, the value of V_{fle}/V_{fix} remains stable and no longer decreases. For the classical compensated foundation structure, the value of V_{fle}/V_{fix} does not decrease after reaching 0.395, while for the piled foundation structure, this value is 1.046. Therefore, current seismic codes may determine whether the V should be reduced and specify different minimum values of reduced shear force depending on the type of foundation.

Moreover, straight line fittings were also performed on the descending sections in Figure 27. The fitting results of the classical compensated foundation structure (Equation (4)) and piled foundation structure (Equation (5)) are as follows, respectively:

$$V_{fle}/V_{fix} = 11.10 - 9.20\left(T_{fle}/V_{fix}\right) \tag{4}$$

$$V_{fle}/V_{fix} = 11.41 - 9.14\left(T_{fle}/V_{fix}\right) \tag{5}$$

The linear correlation coefficients r = −0.9111 and −0.8811 respectively, indicating the two variables are highly negatively correlated. Therefore, in the structural design process, the designer can easily obtain the value of V_{fle} of frame-core tube structures by calculating the V_{fix} and

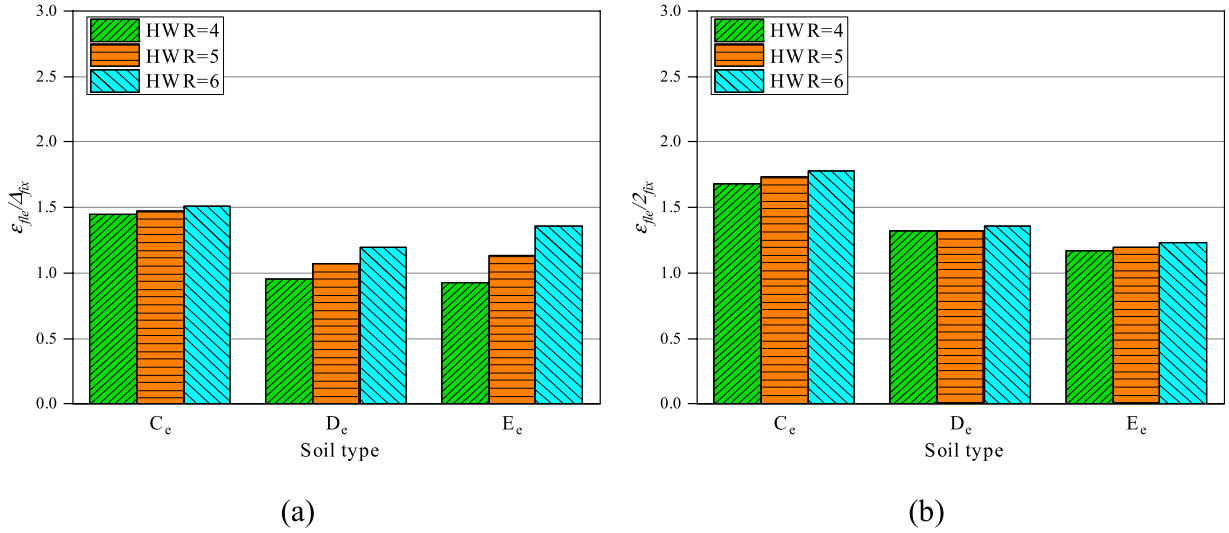

Figure 24. The value of $\delta_{fle}/\delta_{fix}$ of 40-storey frame-core tube structures with different HWRs (a) classical compensated foundation structure (b) piled foundation structure.

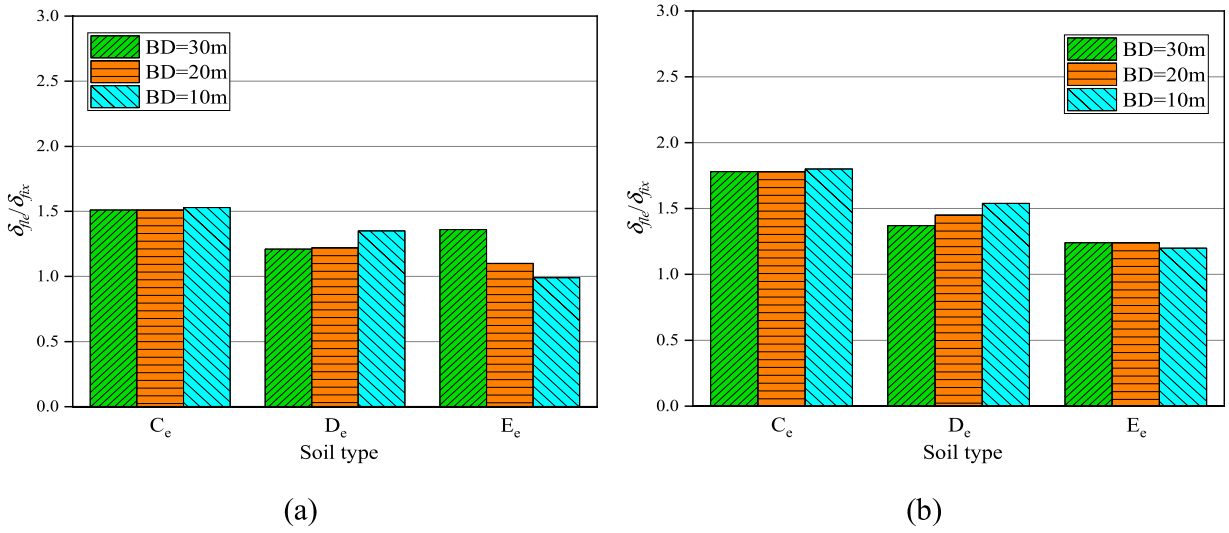

Figure 25. The value of $\delta_{fle}/\delta_{fix}$ of 40-storey frame-core tube structures with different BDs (a) classical compensated foundation structure (b) piled foundation structure.

T_{fle}/T_{fix}, without carrying out time-consuming numerical calculations. In addition, many previous studies have proposed empirical formulas to calculate T_{fle}, which can be found in Balkaya et al. (2012) and Renzi et al. (2013).

Effects of parameters on frame-shear wall structures

The value of V_{fle}/V_{fix} of frame-shear wall structures with different superstructure and substructure parameters are shown in Figures 28–33. Similar to the frame-core tube structure, the values of V_{fle}/V_{fix} increase dramatically with the increase of soil stiffness, and the effects of HWR and BD are much smaller. Moreover, under the conditions of the same foundation and subsoil types, the impact of SSI on the frame-shear wall structures is almost the same as the frame-core tube structure.

The values of $\delta_{fle}/\delta_{fix}$ are shown in Figures 34–39. It also can be found that the value of $\delta_{fle}/\delta_{fix}$ is greater than one in almost all cases. Figure 40 illustrates the relationship between $\delta_{fle}/\delta_{fix}$, V_{fle}/V_{fix} and Δ_θ/Δ. When the values of Δ_θ/Δ are small (less than 0.5 for classical compensated foundation structures and less than 0.15 for piled foundation structures), the data points are basically distributed around the $y=x$ line. As soil stiffness decreases and the values of Δ_θ/Δ become larger, the data points begin to deviate from

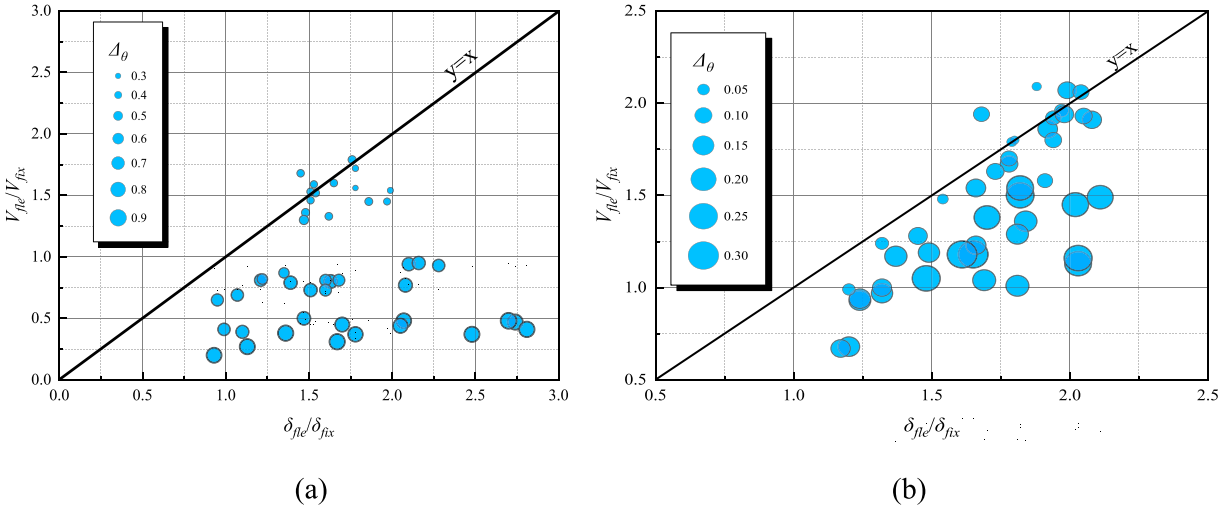

Figure 26. The relationship between $\delta_{fle}/\delta_{fix}$, V_{fle}/V_{fix} and Δ_θ/Δ of frame-core tube structures (a) classical compensated foundation structure (b) piled foundation structure.

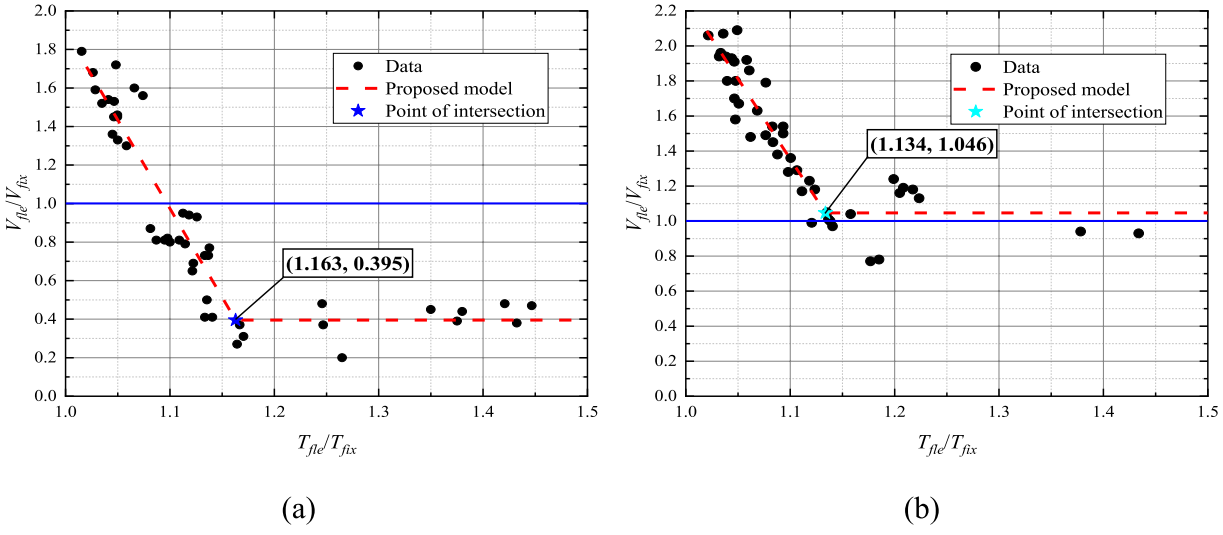

Figure 27. The relationship between T_{fle}/T_{fix} and V_{fle}/V_{fix} of frame-core tube structures (a) classical compensated foundation structure (b) piled foundation structure.

the $y=x$ line and shift downward to the right, indicating that the increase of the value of Δ_θ/Δ tends to amplify the δ and reduce the V of frame-shear wall structures.

Moreover, similar to frame-core tube structures, almost all data points of the pile foundation model lie in the range of $\delta_{fle}/\delta_{fix} > 1$, $V_{fle}/V_{fix}>1$, indicating the SSI has detrimental effects; however, for the classical compensated foundation model, structures with D_e and E_e soil types are below the $V_{fle}/V_{fix}=1$ line, indicating that SSI has a favorable influence, it can reduce the V of the superstructure, even if the inter-storey drifts are still amplified.

Figure 41 shows the relationship between T_{fle}/T_{fix} and V_{fle}/V_{fix}. With the substructure stiffness decreasing and the T_{fle}/T_{fix} increasing, V_{fle}/V_{fix} decreases linearly. But after reaching a certain level, the value of V_{fle}/V_{fix} remains stable and no longer decreases. For the classical compensated foundation structure, the value of V_{fle}/V_{fix} does not decrease after reaching 0.343, while for the piled foundation structure, this value is 0.971. In addition, straight line fittings were also performed on the descending sections in Figure 41. The fitting results of the classical compensated foundation structure (Equation (6)) and piled foundation structure (Equation (7)) are as follows, respectively:

$$V_{fle}/V_{fix} = 10.36 - 8.20\left(T_{fle}/V_{fix}\right) \tag{6}$$

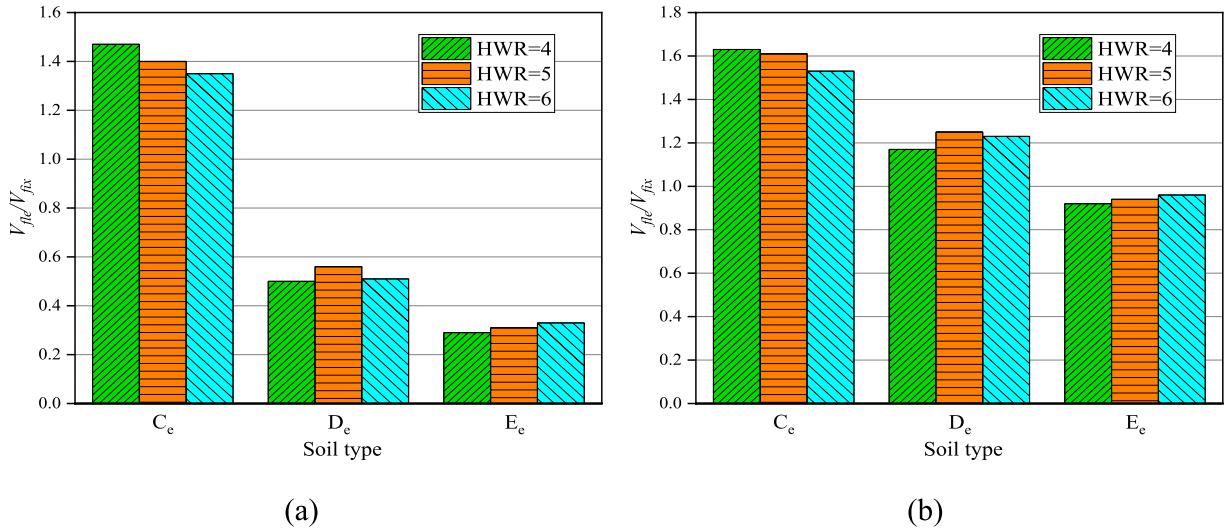

Figure 28. The value of V_{fle}/V_{fix} of 20-storey frame-shear wall structures with different HWRs (a) classical compensated foundation structure (b) piled foundation structure.

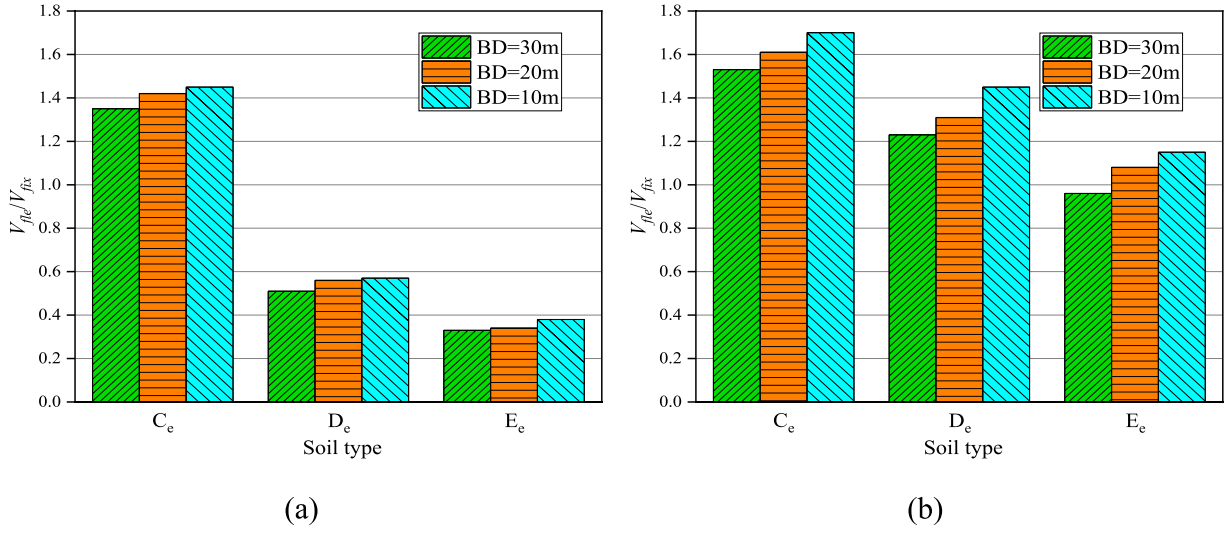

Figure 29. The value of V_{fle}/V_{fix} of 20-storey frame-shear wall structures with different BDs (a) classical compensated foundation structure (b) piled foundation structure.

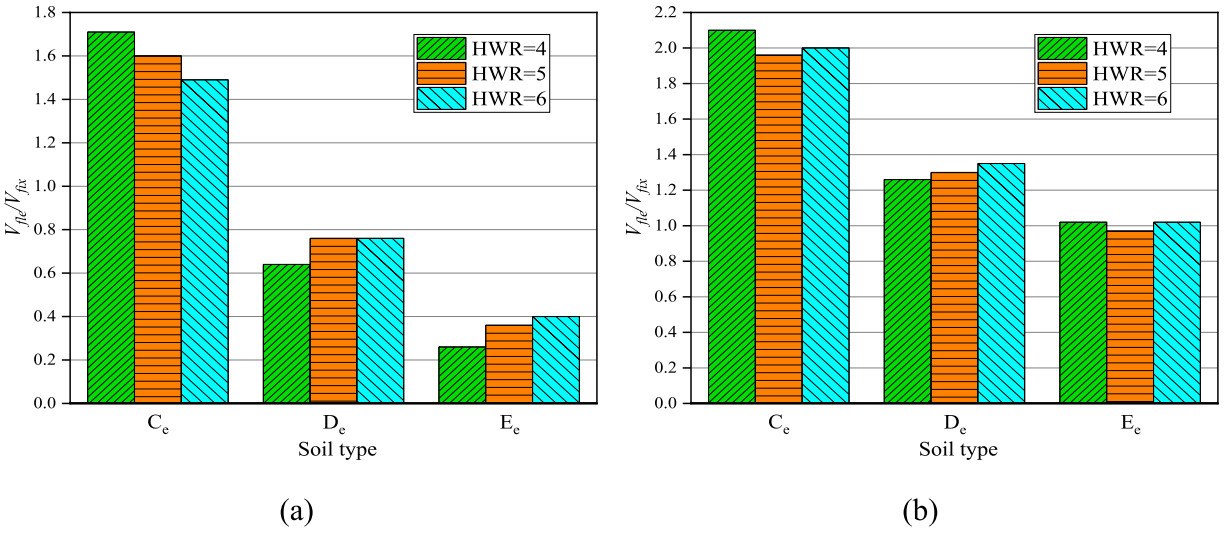

Figure 30. The value of V_{fle}/V_{fix} of 30-storey frame-shear wall structures with different HWRs (a) classical compensated foundation structure (b) piled foundation structure.

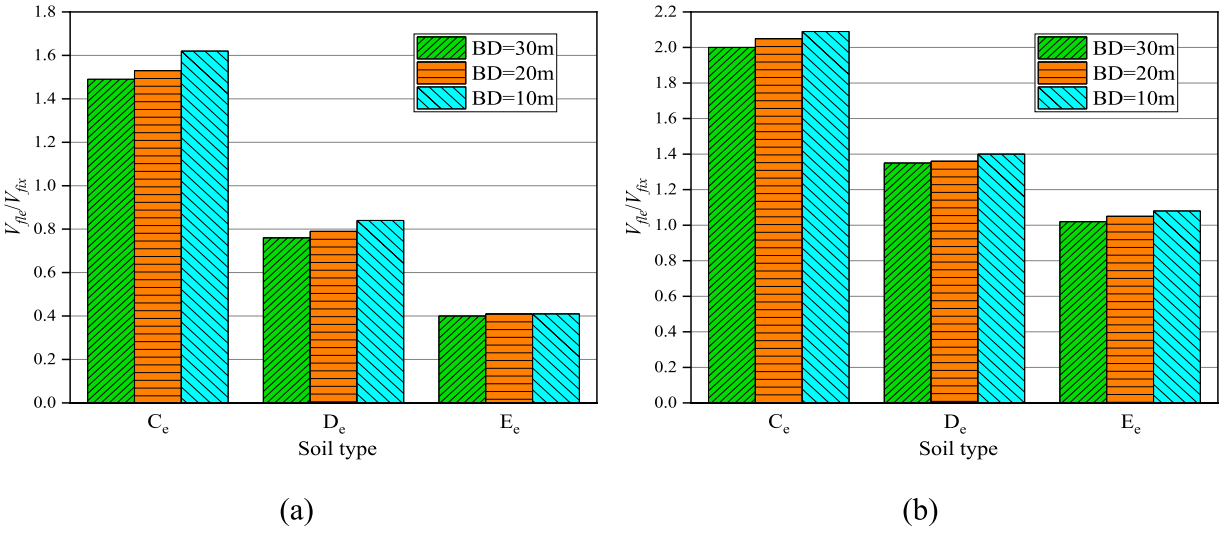

Figure 31. The value of V_{fle}/V_{fix} of 30-storey frame-shear wall structures with different BDs (a) classical compensated foundation structure (b) piled foundation structure.

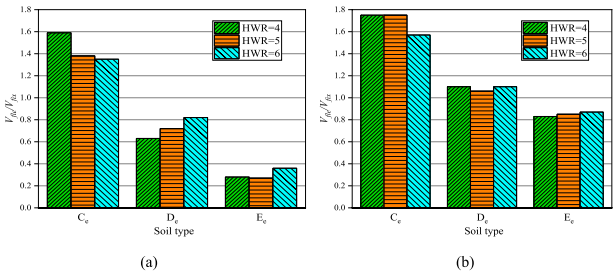

Figure 32. The value of V_{fle}/V_{fix} of 40-storey frame-shear wall structures with different HWRs (a) classical compensated foundation structure (b) piled foundation structure.

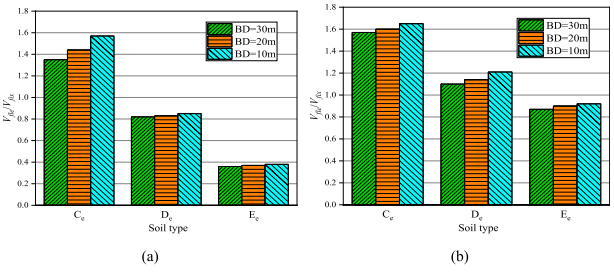

Figure 33. The value of V_{fle}/V_{fix} of 40-storey frame-shear wall structures with different BDs (a) classical compensated foundation structure (b) piled foundation structure.

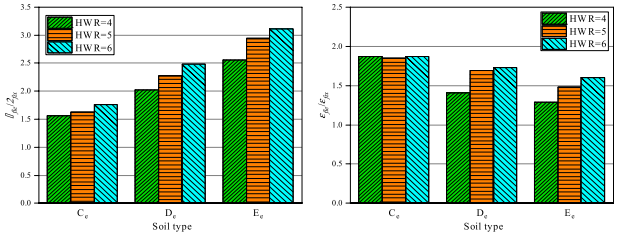

Figure 34. The value of $\delta_{fle}/\delta_{fix}$ of 20-storey frame-shear wall structures with different HWRs (a) classical compensated foundation structure (b) piled foundation structure.

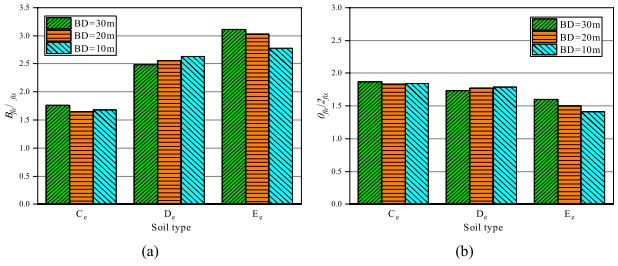

Figure 35. The value of $\delta_{fle}/\delta_{fix}$ of 20-storey frame-shear wall structures with different BDs (a) classical compensated foundation structure (b) piled foundation structure.

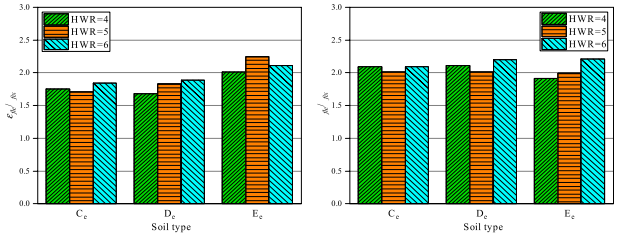

Figure 36. The value of $\delta_{fle}/\delta_{fix}$ of 30-storey frame-shear wall structures with different HWRs (a) classical compensated foundation structure (b) piled foundation structure.

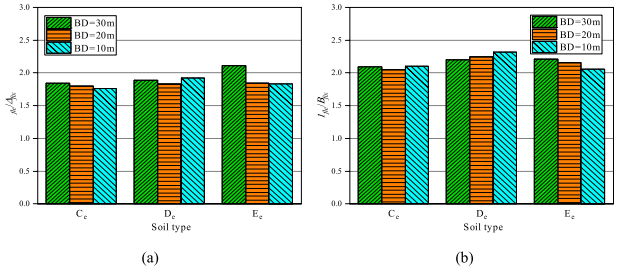

Figure 37. The value of $\delta_{fle}/\delta_{fix}$ of 30-storey frame-shear wall structures with different BDs (a) classical compensated foundation structure (b) piled foundation structure.

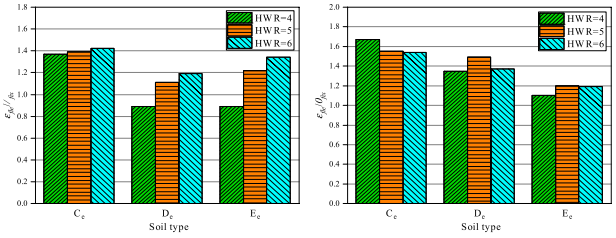

Figure 38. The value of $\delta_{fle}/\delta_{fix}$ of 40-storey frame-shear wall structures with different HWRs (a) classical compensated foundation structure (b) piled foundation structure.

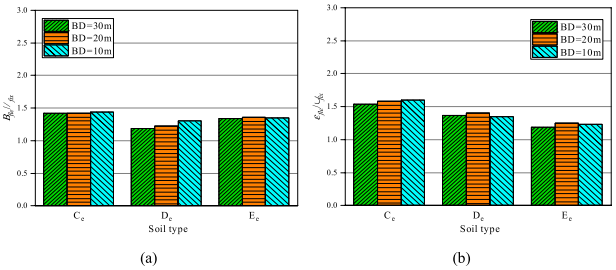

Figure 39. The value of $\delta_{fle}/\delta_{fix}$ of 40-storey frame-shear wall structures with different BDs (a) classical compensated foundation structure (b) piled foundation structure.

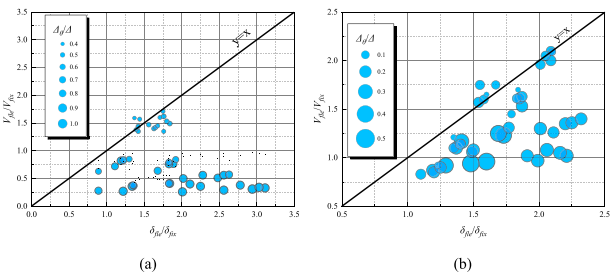

Figure 40. The relationship between $\delta_{fle}/\delta_{fix}$, V_{fle}/V_{fix} and Δ_θ/Δ of frame-shear wall structures (a) classical compensated foundation structure (b) piled foundation structure.

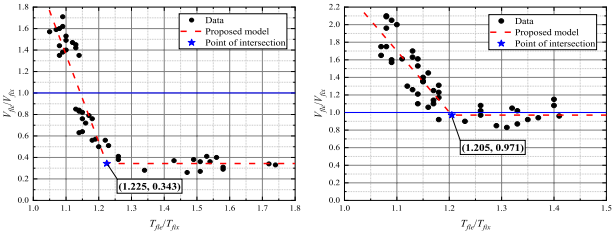

Figure 41. The relationship between T_{fle}/T_{fix} and V_{fle}/V_{fix} of frame-shear wall structures (a) classical compensated foundation structure (b) piled foundation structure.

$$V_{fle}/V_{fix} = 9.85 - 7.43\left(T_{fle}/V_{fix}\right) \quad (7)$$

The linear correlation coefficients r = −0.8731 and −0.8380 respectively, indicating the two variables are highly negatively correlated. Therefore, in the structural design process, designers can easily obtain the value of V_{fle} for frame-shear wall structures by calculating the V_{fix} and T_{fle}/T_{fix}, without carrying out time-consuming numerical calculations.

Conclusions

The objective of this study was to introduce and discuss the effects of various superstructure and substructure parameters (HWR, foundation type, soil type and BD) on the seismic behaviour of tall buildings with different structural systems and heights considering SSI. The governing factors including V and δ of fixed-base and flexible-base structures are obtained and compared to identify the beneficial and detrimental effects of SSI. Based on the results of parametric study, the main conclusions can be obtained as follows.

- Regardless of the structural system and foundation type, the increase of the stiffness of subsoil can significantly increase the value of V_{fle}/V_{fix} of structures. In contrast, HWR and BD has little effect on this value.
- SSI amplifies the value of $\delta_{fle}/\delta_{fix}$ of almost all the cases considered in this study. Therefore, the influence of SSI is detrimental to the δ of tall buildings.
- The influence of the investigated parameters on the value of $\delta_{fle}/\delta_{fix}$ is very complex. In general, the increase of Δ_θ/Δ can amplify the δ and reduce the V.
- SSI amplifies the value of V_{fle}/V_{fix} of piled foundation structures and C_e soil-supported classical compensated foundation structures. In terms of classical compensated foundation structures with D_e and E_e soil types, the impacts of SSI are beneficial because V_{fle}/V_{fix} is reduced.
- With the increase of the T_{fle}/T_{fix}, the value of V_{fle}/V_{fix} decreases linearly until it reaches a specific value. After that, the value of V_{fle}/V_{fix} remains constant. Therefore, current seismic codes may determine whether shear forces should be reduced and specify different minimum values of reduced shear force according to the type of structural system and foundation.

Declaration of conflicting interests

The author(s) declared no potential conflicts of interest with respect to the research, authorship, and/or publication of this article.

Funding

The author(s) received no financial support for the research, authorship, and/or publication of this article.

ORCID iD

Xiaofeng Zhang https://orcid.org/0009-0008-0354-6398

References

Al Agha W, Alozzo Almorad W, Umamaheswari N, et al. (2021) Study the seismic response of reinforced concrete high-rise building with dual framed-shear wall system considering the effect of soil structure interaction. *Materials Today: Proceedings* 43: 2182–2188.

Anand V and Satish Kumar SR (2018) Seismic soil-structure interaction: a state-of-the-art review. *Structures* 16: 317–326.

Ansari M, Nazari M and Panah AK (2021) Influence of foundation flexibility on seismic fragility of reinforced concrete high-rise buildings. *Soil Dynamics and Earthquake Engineering* 142: 106521.

Arboleda-Monsalve LG, Mercado JA, Terzic V, et al. (2020) Soil-structure interaction effects on seismic performance and earthquake-induced losses in tall buildings. *Journal of Geotechnical and Geoenvironmental Engineering* 146(5): 04020028.

AS1170.4 (2007) *Structural Design Actions: Part 4: Earthquake Actions in Australia*. Sydney: Australian standards.

AS3600 (2018) *Concrete Structures*. Sydney: Australian standards.

Ayala F, Sáez E and Magna-Verdugo C (2022) Computational modelling of dynamic soil-structure interaction in shear wall buildings with basements in medium stiffness sandy soils using a subdomain spectral element approach calibrated by micro-vibrations. *Engineering Structures* 252: 113668.

Bagheri M, Jamkhaneh ME and Samali B (2018) Effect of seismic soil-pile-structure interaction on mid-and high-rise steel buildings resting on a group of pile foundations. *International Journal of Geomechanics* 18(9): 04018103.

Balkaya C, Yuksel SB and Derinoz O (2012) Soil-structure interaction effects on the fundamental periods of the shear-wall dominant buildings. *The Structural Design of Tall and Special Buildings* 21(6): 416–430.

Bryce T, Far H and Gardner A (2019) Barriers to career advancement for female engineers in Australia's civil construction industry and recommended solutions. *Australian Journal of Civil Engineering* 17(1): 1–10.

Carbonari S, Dezi F and Leoni G (2011) Linear soil-structure interaction of coupled wall-frame structures on pile foundations. *Soil Dynamics and Earthquake Engineering* 31(9): 1296–1309.

Carbonari S, Dezi F and Leoni G (2012) Nonlinear seismic behaviour of wall-frame dual systems accounting for soil-structure interaction. *Earthquake Engineering & Structural Dynamics* 41(12): 1651–1672.

Dassault Systèmes SIMULIA (2012) *Abaqus Analysis User's Manual*. Minneapolis: Dassault Systèmes SIMULIA Corporation.

Far H (2019) Dynamic behaviour of unbraced steel frames resting on soft ground. *Steel Construction* 12(2): 135–140.

Far H (2020) Flexural behavior of cold-formed steel-timber composite flooring systems. *Journal of Structural Engineering* 146(5): 0602000312.

Far H and Flint D (2017) Significance of using isolated footing technique for residential construction on expansive soils. *Frontiers of Structural and Civil Engineering* 11(1): 123–129.

Fatahi B and Tabatabaiefar HR (2014) Effects of soil plasticity on seismic performance of mid-rise building frames resting on soft soils. *Advances in Structural Engineering* 17(10): 1387–1402.

Tabatabaiefar HR, Fatahi B, Ghabraie K, et al. (2015) Evaluation of numerical procedures to determine seismic response of structures under influence of soil-structure interaction. *Structural Engineering & Mechanics* 56(1): 27–47.

Fathi A, Sadeghi A, Emami Azadi MR, et al. (2020) Assessing the soil-structure interaction effects by direct method on the out-of-plane behavior of masonry structures (case study: Arge-Tabriz). *Bulletin of Earthquake Engineering* 18(14): 6429–6443.

Galal K and Naimi M (2008) Effect of soil conditions on the response of reinforced concrete tall structures to near-fault earthquakes. *The Structural Design of Tall and Special Buildings* 17(3): 541–562.

Gao L, Fang E and Qian J (2005) *Conceptual Design of High-Rise Building Structure*. Beijing: China Planning Press.

Gazetas G (1983) Analysis of machine foundation vibrations: state of the art. *International Journal of Soil Dynamics and Earthquake Engineering* 2(1): 2–42.

Ghandil M and Behnamfar F (2017) Ductility demands of MRF structures on soft soils considering soil-structure interaction. *Soil Dynamics and Earthquake Engineering* 92: 203–214.

Gu Y, Liu JB and Du YX (2007) 3D consistent viscous-spring artificial boundary and viscous-spring boundary element. *Engineering Mechanics* 24(12): 31–37.

Haydar H, Far H and Saleh A (2018) Portal steel trusses vs. portal steel frames for long-span industrial buildings. *Steel Construction* 11(3): 205–217.

Hokmabadi AS, Fatahi B and Samali B (2012) Recording inter-storey drifts of structures in time-history approach for seismic design of building frames. *Australian Journal of Structural Engineering* 13(2): 175–179.

Hokmabadi AS, Fatahi B and Samali B (2014) Assessment of soil-pile-structure interaction influencing seismic response of mid-rise buildings sitting on floating pile foundations. *Computers and Geotechnics* 55: 172–186.

Hokmabadi AS, Fatahi B and Samali B (2015) Physical modeling of seismic soil-pile-structure interaction for buildings on soft soils. *International Journal of Geomechanics* 15(2): 04014046.

Kamal M, Inel M and Cayci BT (2022) Seismic behavior of mid-rise reinforced concrete adjacent buildings considering soil-structure interaction. *Journal of Building Engineering* 51: 104296.

Karapetrou ST, Fotopoulou SD and Pitilakis KD (2015) Seismic vulnerability assessment of high-rise non-ductile RC buildings considering soil–structure interaction effects. *Soil Dynamics and Earthquake Engineering* 73: 42–57.

Karki D, Far H and Saleh A (2021) Numerical studies into factors affecting structural behaviour of composite cold-formed steel and timber flooring systems. *Journal of Building Engineering* 44: 102692.

Kramer SL (1996) *Geotechnical Earthquake Engineering*. Upper Saddle River: Prentice Hall.

Liang J, Zhang G, Ba Z, et al. (2023) Seismic response analysis of high-rise frame-core tube building on fluid-saturated soil considering soil-pile-structure interaction. *Journal of Building Engineering* 63: 105563.

Lin X, Far H and Saleh A (2019) Structural behaviour and mechanical properties of welded steel I-girders with corrugated webs. *International Journal of Steel Structures* 19(4): 1342–1352.

Liu JB, Du YX, Du XL, et al. (2006) 3D viscous-spring artificial boundary in time domain. *Earthquake Engineering and Engineering Vibration* 5(1): 93–102.

Liu ST, Li PZ, Zhang WY, et al. (2020) Experimental study and numerical simulation on dynamic soil-structure interaction under earthquake excitations. *Soil Dynamics and Earthquake Engineering* 138: 106333.

Lu Y (2005) Inelastic behaviour of RC wall-frame with a rocking wall and its analysis Incorporating 3-D effect. *The Structural Design of Tall and Special Buildings* 14(1): 15–35.

Ma SJ, Chi MJ, Chen HJ, et al. (2020) Implementation of viscous-spring boundary in ABAQUS and comparative study on seismic motion input methods. *Chinese Journal of Rock Mechanics and Engineering* 39(7): 1445–1457.

Meymand PJ (1998) *Shaking Table Scale Model Tests of Nonlinear Soil-Pile Superstructure Interaction in Soft Clay*. Berkeley: University of California.

Nasab MSE, Chun S and Kim J (2021) Soil-structure interaction effect on seismic retrofit of a soft first-story structure. *Structures* 32: 1553–1564.

Park D and Hashash YMA (2004) Soil damping formulation in nonlinear time domain site response analysis. *Journal of Earthquake Engineering* 8(2): 249–274.

Qaftan OS, Toma-Sabbagh T, Weekes L, et al. (2020) Validation of a finite element modelling approach on soil-foundation-structure interaction of a multi-storey wall-frame structure under dynamic loadings. *Soil Dynamics and Earthquake Engineering* 131: 106041.

Rayhani M and El Naggar MH (2008) Numerical modeling of seismic response of rigid foundation on soft soil. *International Journal of Geomechanics* 8(6): 336–346.

Renzi S, Madiai C and Vannucchi G (2013) A simplified empirical method for assessing seismic soil-structure interaction effects on ordinary shear-type buildings. *Soil Dynamics and Earthquake Engineering* 55: 100–107.

Saleh A, Far H and Mok L (2018) Effects of different support conditions on experimental bending strength of thin walled cold formed steel storage upright frames. *Journal of Constructional Steel Research* 150: 1–6.

Samanta A and Swain A (2019) Seismic response and vulnerability assessment of representative low, medium and high-rise buildings in Patna, India. *Structures* 19: 110–127.

Scarfone R, Morigi M and Conti R (2020) Assessment of dynamic soil-structure interaction effects for tall buildings: a 3D numerical approach. *Soil Dynamics and Earthquake Engineering* 128: 105864.

Seed HB, Wong R, Idriss IM, et al. (1986) Moduli and damping factors for dynamic analyses of cohesionless soils. *Journal of Geotechnical Engineering* 112(11): 1016–1032.

Segaline H, Sáez E and Ubilla J (2022) Evaluation of dynamic soil-structure interaction effects in buildings with underground stories using 1 g physical experimentation in a transparent shear laminar box. *Engineering Structures* 266: 114645.

Son H, Park J, Kim H, et al. (2017) Generalized finite element analysis of high-rise wall-frame structural systems. *Engineering Computations* 34(1): 189–210.

Sun JI, Golesorkhi R and Seed B (1998) *Dynamic Module and Damping Ratios for Cohesive Soils. Earthquake Engineering Research Centre, Report No. UCB/EERC-88/15*. Berkeley: University of California.

Tabatabaiefar HR (2016) Detail design and construction procedure of laminar soil containers for experimental shaking table tests. *International Journal of Geotechnical Engineering* 10(4): 328–336.

Tabatabaiefar HR and Clifton T (2016) Significance of considering soil-structure interaction effects on seismic design of unbraced building frames resting on soft soils. *Australian Geomechanics Journal* 51(1): 55–64.

Tabatabaiefar HR and Fatahi B (2014) Idealisation of soil-structure system to determine inelastic seismic response of mid-rise building frames. *Soil Dynamics and Earthquake Engineering* 66: 339–351.

Tabatabaiefar HR and Mansoury B (2016) Detail design, building and commissioning of tall building structural models for experimental shaking table tests. *The Structural Design of Tall and Special Buildings* 25(8): 357–374.

Tabatabaiefar HR and Massumi A (2010) A simplified method to determine seismic responses of reinforced concrete moment resisting building frames under influence of soil-structure interaction. *Soil Dynamics and Earthquake Engineering* 30(11): 1259–1267.

Tabatabaiefar HR, Fatahi B and Samali B (2013) Seismic behaviour of building frames considering dynamic soil-structure interaction. *International Journal of Geomechanics* 13(4): 409–420.

Tabatabaiefar HR, Fatahi B and Samali B (2014a) Numerical and experimental investigations on seismic response of building frames under influence of soil-structure interaction. *Advances in Structural Engineering* 17(1): 109–130.

Hamid Reza Tabatabaiefar S, Fatahi B and Samali B (2014b) An empirical relationship to determine lateral seismic response of mid-rise building frames under influence of soil-structure interaction. *The Structural Design of Tall and Special Buildings* 23(7): 526–548.

Van Nguyen Q, Fatahi B and Hokmabadi AS (2017) Influence of size and load-bearing mechanism of piles on seismic performance of buildings considering soil-pile-structure interaction. *International Journal of Geomechanics* 17(7): 04017007.

Wang J and Yang J (2022) Parametric analysis on the effect of dynamic interaction between nonlinear soil and reinforced concrete frame. *Applied Sciences* 12: 9876.

Wolf JP (1985) *Dynamic Soil-Structure Interaction*. Englewood Cliffs, New Jersey: Prentice-Hall.

Wolf JP and Deeks AJ (2004) *Foundation Vibration Analysis: A Strength Of-Materials Approach*. Oxford: Elsevier.

Yang JP, Lu Z and Li PZ (2020) Large-scale shaking table test on tall buildings with viscous dampers considering pile-soil-structure interaction. *Engineering Structures* 220: 110960.

Yeganeh N, Bolouri Bazaz J and Akhtarpour A (2015) Seismic analysis of the soil-structure interaction for a high rise building adjacent to deep excavation. *Soil Dynamics and Earthquake Engineering* 79: 149–170.

Zhang X and Far H (2022) Effects of dynamic soil-structure interaction on seismic behaviour of high-rise buildings. *Bulletin of Earthquake Engineering* 20(7): 3443–3467.

Zhang W, Liu S, Shokrabadi M, et al. (2022) Nonlinear seismic fragility assessment of tall buildings equipped with tuned mass damper (TMD) and considering soil-structure interaction effects. *Bulletin of Earthquake Engineering* 20(7): 3469–3483.